Genetic variation in the species *Arabidopsis thaliana* reveals the existence of natural heat resilience factors for meiosis

Jiayi Zhao[1], Huiqi Fu[1], Zhengze Wang[2], Min Zhang[1], Yaoqiong Liang[1], Xueying Cui[1], Wenjing Pan[1], Ziming Ren[3], Zhihua Wu[4], Yujie Zhang[1], Xin Gui[1], Li Huo[1], Xiaoning Lei[5], Chong Wang[6], Arp Schnittger[7], Wojciech P. Pawlowski[8], Bing Liu[1,✉]

[1]Arameiosis Lab, South-Central Minzu University, Wuhan 430074;

[2]College of Life Science and Technology, Huazhong Agricultural University, Wuhan 430070;

[3]Department of Landscape Architecture, Zhejiang Sci-Tech University, Hangzhou 310018;

[4]College of Life Sciences, Zhejiang Normal University, Jinhua 321004;

[5]School of Public Health, Shanghai Jiao Tong University School of Medicine, Shanghai 200025;

[6]Shanghai Key Laboratory of Plant Molecular Sciences, Development Center of Plant Germplasm Resources, College of Life Sciences, Shanghai Normal University, Shanghai 200234;

[7]Department of Developmental Biology, University of Hamburg, Hamburg 22609;

[8]School of Integrative Plant Science, Cornell University, Ithaca, NY 14853;

✉To whom correspondence should be addressed: B.L. (arameiosis@163.com).

ORCID

Arp Schnittger: 0000-0001-7067-0091

Wojciech P. Pawlowski: 0000-0003-0770-2083

Bing Liu: 0000-0002-8547-0970

Short title: Natural genetic variation controls heat tolerance of meiosis in Arabidopsis

One-sentence summary: *Arabidopsis thaliana* reveals accession-specific heat tolerance of meiosis that is controlled by multiple genomic loci derived from natural variations.

Total wordcount (Introduction, Materials and Methods, Results and Discussion): 5736

Discussion section: 1122 (19.6% of the total wordcount)

Numbers of figures: 9 (all in color)

Summary

- Heat interferes with multiple meiotic processes leading to genome instability and sterility in flowering plants, including many crops. Despite its importance for food security, the mechanisms underlying heat tolerance of meiosis are poorly understood.
- We analyzed different meiotic processes in the Arabidopsis (*Arabidopsis thaliana*) accessions Columbia (Col) and Landsberg *erecta* (L*er*), their F1 hybrids and F2 offspring under heat stress (37°C).
- At 37°C, Col exhibits significantly reduced formation of double-stand breaks (DSBs) and completely abolished homolog pairing, synapsis and crossover (CO) formation. Strikingly, L*er* and L*er*/Col hybrids are much less affected than Col. Interestingly, only 10% ~ 20% of F2 offspring exhibit the same heat tolerance of meiotic recombination as parents, indicating that heat resilience in L*er* is controlled by the interplay of several loci.
- This study reveals the existence of natural heat resilience factors for meiosis in Arabidopsis, which have the great potential to be exploited in breeding programs.

Keywords

Meiosis, heat stress, meiotic recombination, homolog pairing, crossover, genetic variation, *Arabidopsis thaliana*

Introduction

Meiosis is a specialized type of cell division, which, in plants, generates spores with halved chromosome number required for sexual reproduction and maintenance of ploidy consistency over generations. During prophase I, homologous chromosomes (homologs) undergo recombination, resulting in reciprocal exchange of DNA fragments and thereby promoting genetic diversity. Meiotic recombination is initiated by the programmed formation of DNA double-strand breaks (DSBs) catalyzed by the conserved topoisomerase VI-like protein SPO11 together with other components of the DSB formation machinery (Vrielynck *et al.*, 2021; Nore *et al.*, 2022). The recombinases RAD51 and DMC1 catalyze DSB repair via homologous recombination (Kurzbauer *et al.*, 2012; Da Ines *et al.*, 2013; Chen, H *et al.*, 2021). In plants, deficiencies in DSB repair result in impaired crossover (CO) formation and/or cause chromosome fragmentation (Kurzbauer *et al.*, 2012; Da Ines *et al.*, 2013; Su *et al.*, 2017; Chen, H *et al.*, 2021). Although a large

number of DSBs is generated along chromosomes, only a small proportion of them are repaired into COs. In Arabidopsis as in many other species, most COs are catalyzed by the ZMM proteins resulting in type-I COs that are placed with a distance to each other (CO interference) (Ziolkowski, 2023). The formation of the remaining approximately 15% of COs in plants involves structure-selective endonucleases such as MUS81 giving rise to type-II COs, which are typically not subject to CO interference (Wang & Copenhaver, 2018). The process of COs formation can be visualized by the linking of homologs giving rise to bivalents connected by chiasmata. In the wild-type, all homologs become eventually connected through at least one CO (CO assurance) (Jones & Franklin, 2006), which is required for equal distribution of homologs after meiosis I.

During meiotic recombination, chromatids are organized into loops, the basal regions of which are anchored to an axis through the interactions between axis core proteins (e.g. ASY3 and ASY4 in Arabidopsis) and the axis-associated HORMA domain protein ASY1 (Armstrong *et al.*, 2002; Ferdous *et al.*, 2012; Chambon *et al.*, 2018; West *et al.*, 2019). The assembly of the chromosome axis is required for normal DSB formation and repair, homolog pairing and synapsis, and recombination (Ferdous *et al.*, 2012; Lambing, Christophe *et al.*, 2020; Lambing, C. *et al.*, 2020; Yang *et al.*, 2022).

The separation of homologs and sister chromatids is facilitated by spindles. Cohesin, a ring-shaped protein complex, assures the protection of the sister-chromatids union. The cohesion on chromosome arms is released during prophase and particularly during anaphase I allowing the separation of homologs (Yang *et al.*, 2019). The centromeric cohesion is removed in anaphase II paving the road for the segregation of sister chromatids (Onn *et al.*, 2008). The function and stability of centromeres are crucial for maintenance of cohesion and thus faithful chromosome segregation (McKinley & Cheeseman, 2016; Chen, Y. *et al.*, 2021).

Several studies have shown that meiosis in plants is sensitive to temperature variations (Bomblies *et al.*, 2015; Modliszewski & Copenhaver, 2017; Liu *et al.*, 2019; De Jaeger-Braet *et al.*, 2022; De Jaeger-Braet & Schnittger, 2024). Either elevated or reduced temperature can interfere with cytoskeleton organization and/or meiotic cell cycle transition resulting in defective cytokinesis and unreduced spores (Tang *et al.*, 2011; De Storme *et al.*, 2012; Liu *et al.*, 2018; De Storme & Geelen, 2020; Zhou *et al.*, 2022). In Arabidopsis, mildly decreased or increased temperature within the spectrum that does not reduce fertility (8-28°C) promotes type-I CO formation (Lloyd *et al.*, 2018; Modliszewski *et al.*, 2018). Higher temperatures (30-34°C), however, attenuate homolog synapsis and alter CO rate and distribution, affecting meiosis progression (De Storme & Geelen, 2020; De Jaeger-Braet *et al.*, 2022). In addition, increased

90 temperatures perturb stability of centromeres and induce unbalanced chromosome segregation in Arabidopsis
91 (Ahmadli *et al.*, 2023; Jin *et al.*, 2023; Crhak Khaitova *et al.*, 2024). At extremely high temperatures (36-38°C), homolog
92 pairing and synapsis and CO formation in the Arabidopsis accession Columbia (Col) is completely abolished, which
93 results in disrupted chromosome segregation and sterility (Lei *et al.*, 2020; Ning *et al.*, 2021; Fu *et al.*, 2022). Despite
94 the significance of heat stress on genetic makeup and genome stability in plants, the molecular mechanisms controlling
95 heat tolerance of meiosis remain poorly understood.
96
97 Interestingly, previous studies have shown that there are naturally existing genetic differences with respect to meiotic
98 recombination and stress tolerance in plants (Schulz *et al.*, 2015; Sidhu *et al.*, 2015; Ziolkowski *et al.*, 2017; Taghavi
99 Namin *et al.*, 2018; Lardon *et al.*, 2020; Chen, Ying *et al.*, 2021; Zhu *et al.*, 2021). Here, we report that the *Arabidopsis*
100 *thaliana* accessions Col and Landsberg *erecta* (L*er*) have striking differences in heat tolerance of meiotic recombination.
101 Our data reveal that meiotic chromosome stability in Col/L*er* F2 progeny is more sensitive to heat than in either inbreds
102 or their hybrids indicating that several loci contribute to the natural heat resistance.
103
104 **Material and Methods**
105
106 **Plant materials and growth conditions**
107
108 *Arabidopsis thaliana* (L.) accessions Columbia (Col-0) and Landsberg *erecta* (L*er*), the *atm-2* (Kurzbauer *et al.*, 2021),
109 *atm-5* (Yao *et al.*, 2020), *er-105*, *mpk6*, *er-105 mpk6* (Cai *et al.*, 2017), *dmc1* (Couteau et al., 1999), *spo11-1-3* (Xue *et*
110 *al.*, 2018), *msh4* (Higgins *et al.*, 2004) and *zyp1a/b* (Yang *et al.*, 2022) mutants were used in this study. Col/L*er* hybrids
111 were obtained by crossing using L*er* as pollen donator. The bi-allelic mutant $ATM^{atm\text{-}2/atm\text{-}5}$ was obtained by crossing the
112 heterozygous *atm-2* and *atm-5* mutants. Genotyping was performed using the primers listed in Table S1. Arabidopsis
113 were cultivated in a growth chamber with a 16 h day/8 h night and 20°C condition. For heat treatment, young flowering
114 plants were treated by 37°C for 24 h in a humid chamber with a 16 h day/8 h night condition. To avoid potential impact
115 of circadian clock, heat treatment was applied starting from 8:00-10:00 am.
116
117 **Cytological analysis of meiocytes**
118
119 After heat treatment, plants were transferred back to 20°C for 6-12 h recovery, and tetrad stage meiocytes were

120 analyzed (Lei *et al.*, 2020). A drop of 4.5% (w/v) lactopropionic orcein staining buffer was added to the surface of a
121 tetrad-staged flower bud (floral bud stage 9, 0.3-0.4 mm) (Armstrong & Jones, 2003) followed by squashing to release
122 meiocytes.
123
124 **Preparation of chromosome spreads**
125
126 Inflorescences were isolated and fixed in cold Carnoy's fixative for at least 24 h. Flower buds at stages beyond tetrads
127 were removed, and the remaining buds were washed twice in distilled water and once in citrate buffer (10 mM, pH =
128 4.5), followed by incubation in a digestion enzyme mixture (0.3% pectolyase and 0.3% cellulase in citrate buffer) at
129 37°C for 3 h. Digested flower buds were subsequently washed once in distilled water, which thereafter were macerated
130 in distilled water on a glass slide. Two rounds of 60% acetic acid were added to the slide, which was dried on a hotplate
131 at 45°C. The slide was flooded with cold Carnoy's fixative and then was air dried. 4',6-diamidino-2-phenylindole (DAPI)
132 was diluted to 5 μg/mL in Vectashield antifade mounting media (Vector Laboratories).
133
134 **Immunolocalization of α-tubulin and meiotic recombination proteins**
135
136 To perform immunolocalization of α-tubulin, inflorescences were fixed by 4% (w/v) paraformaldehyde under vacuum
137 for 30 min, followed by twice washes in distilled water and once in citrate buffer (10 mM, pH = 6.0). Meiosis-staged
138 flower buds were digested in an enzyme mixture consisting of 0.3% (w/v) cellulase (Sigma), 0.3% (w/v) pectolyase
139 (Sigma) and 0.3% (w/v) cytohelicase (Sigma) in a humid chamber at 37°C for 3 h. After the digestion, anthers were
140 dissected, squashed, and fixed on a slide by freezing in liquid nitrogen. Released cells on the slide were immobilized
141 with a thin layer of gel containing 1% (w/v) gelatin, 1% (w/v) agarose and 2.5% (w/v) sucrose. After rinsing with
142 phosphate buffered saline with 1% (v/v) Triton-X 100 for 30 min, the α-tubulin antibody diluted in phosphate buffered
143 saline with 0.1% (v/v) Triton X-100 and 4.5 g/L bovine serum albumin was added and the slide was incubated overnight
144 at 4°C. The slide washed three times with phosphate buffered saline with 0.02% tween-20 was incubated with a
145 secondary antibody at 37°C for 1 h in the dark. Immunolocalization of meiotic recombination proteins was performed
146 as previously described (Chelysheva *et al.*, 2010; Wang *et al.*, 2014), and the antibodies used in this study have been
147 reported previously (Lei *et al.*, 2020; Ning *et al.*, 2021; Zhao *et al.*, 2023).
148
149 **Quantification of fluorescent foci, fluorescence intensity and chromosome fragments**

150

151 Fluorescent images were taken by an Olympus IX83 inverted fluorescence microscope with a X-Cite lamp and a Prime
152 BSI camera, and Z-stacks were processed using ImageJ. The fluorescent foci merged onto DAPI-stained chromosomes
153 were counted. For the pixel intensity plot, the pixel brightness through a region of interest was measured using ImageJ
154 and plotted against the X dimension. To score the number of chromosome fragments, chromosome bodies in
155 meiocytes at metaphase I, anaphase I and metaphase II that were obviously brighter than organelles were counted
156 followed by a subtraction of expected chromosome number (5 at metaphase I, 10 at anaphase I or metaphase II).

157

158 **Statistical analysis**

159

160 Significance was calculated using unpaired *t*-tests (Fig. 1b; Fig. 2c, d, h and j; Fig. 4b, d, and h; Fig. 6d and e; Fig. 7d and
161 g; Fig. 9b and d) or Chi-squared tests (Fig. 1f; Fig. 2f; Fig. 3j, l and t; Fig. 4f, j, l and n; Fig. 7c; Fig. 8c and h; Fig. 9g, h, k
162 and l) with the software GraphPad Prism. The significance level was set as $P < 0.05$. To calculate the frequency of
163 individuals or meiocytes showing either altered chromosome morphology in interkinesis (Fig. 6c, d and e), untimely
164 sister-chromatids segregation, or number of chromosome fragments (Fig. 7c, d and g), the individuals, in which a
165 meiocyte with the corresponding defect was observed, and at least three meiocytes at the corresponding stage were
166 found, were used for calculation. The numbers of analyzed meiocytes or individuals are shown in the figures or main
167 text. Correlation between different meiosis phenotypes was determined based on Spearman's rank correlation tests.
168 Coefficients were calculated using Corrplot package on the R statistical platform, and Ggpubr package was used for
169 visualization.

170

171 **Results**

172

173 **Landsberg *erecta* exhibits higher heat tolerance of meiosis than Columbia**

174

175 The *Arabidopsis thaliana* accessions Columbia (Col) and Landsberg *erecta* (L*er*), two frequently used varieties, exhibit
176 differences in their meiotic recombination rates as well as response to stresses (Schiavon *et al.*, 2007; Lasky *et al.*,
177 2014; Schulz *et al.*, 2015; Ziolkowski *et al.*, 2017; Choi *et al.*, 2019; Chen, Ying *et al.*, 2021). To test whether heat
178 tolerance of meiosis also varies, we compared the effect of extreme heat stress, i.e., 37°C, versus the control condition,
179 i.e., 20°C, between these two accessions. To this end, we analyzed tetrad formation at the end of meiosis by orcein

180 staining. At 20°C, both accessions generated typical tetrads that harbored four spores with equally-sized nuclei (Fig.
181 1a and b). Exposure to the extreme temperature resulted in 85.7% tetrads in Col that showed irregular configurations
182 with abnormal numbers and/or sizes of spores and nuclei (Fig. 1a and b). In striking contrast, only 8.8% abnormal
183 tetrads were found in L*er* (Fig. 1a and b), suggesting that meiosis in L*er* is more resilient to heat stress than Col.
184
185 Heat-induced formation of abnormal tetrads could result from defective meiotic recombination that leads to
186 univalents and consequently, chromosome mis-segregation. Alternatively, defects in microtubule-mediated
187 chromosome distribution and/or cytokinesis could be the underlying cause (Lei *et al.*, 2020). To determine which
188 meiotic process in Col is more affected by heat stress, we analyzed the spindle at metaphase I and II as well as
189 phragmoplast at telophase II (Liu *et al.*, 2017; Liu *et al.*, 2018; Lei *et al.*, 2020). At 20°C, the typical barrel-shaped
190 spindles and straight phragmoplasts were observed in both accessions. (Fig. S1, Fig. 1c). At 37°C, we did not observe
191 obvious defects in microtubule organization in prophase I meiocytes in either accession (Fig. S1) while Col and L*er*
192 showed similar rates of irregularities in morphology of spindles and phragmoplasts in meiosis I and/or II (Fig. 1d,
193 normal; e, abnormal; and f) that likely contributed to an unequal segregation of chromosomes (Fig. 1g). The higher
194 heat tolerance of meiosis in L*er* versus Col is thus likely not caused by the difference in microtubule organization, but
195 possibly occurs prior to metaphase I, i.e., in meiotic recombination.
196

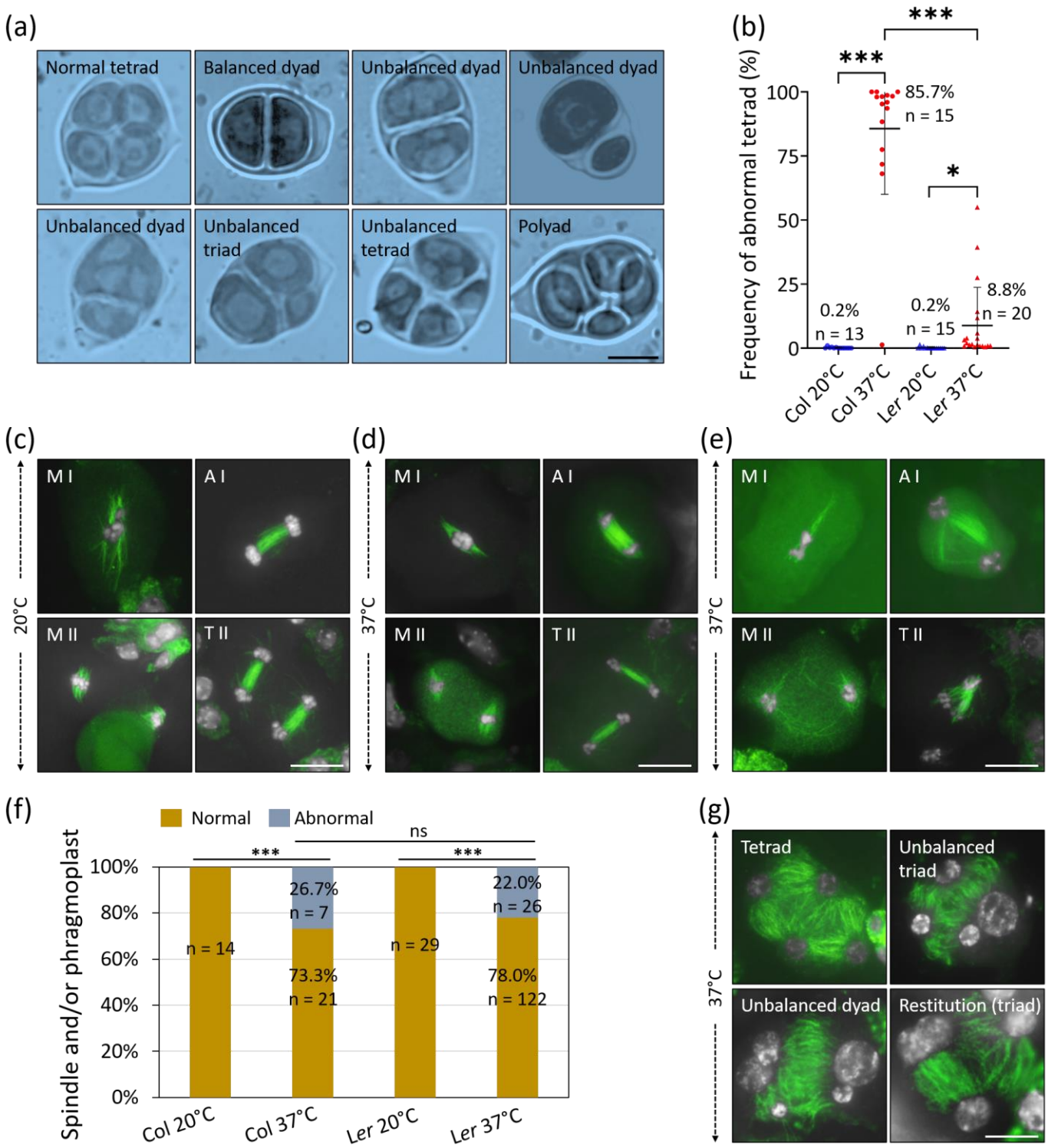

Figure 1. L*er* exhibits a higher heat tolerance of meiosis than Col. (a) Representative images of tetrads with normal or abnormal configurations. (b) Graph showing the frequencies of abnormal tetrads in Col and L*er* at 20°C or 37°C. Stars indicate significance levels based on unpaired *t* tests. (c and d) Representative images of immunolocalization of α-tubulin in metaphase I, anaphase I, metaphase II and telophase II meiocytes depicting normal microtubule configurations at 20°C (c) or 37°C (d). (e) Representative images of immunolocalization of α-tubulin in metaphase I, anaphase I, metaphase II and telophase II meiocytes displaying altered

configurations at 37°C. (f) Graph showing the rates of spindle and phragmoplast with normal or abnormal configurations in Col and L*er* at 20°C or 37°C. Stars indicate significance levels based on χ^2-tests. (g) Representative images of immunolocalization of α-tubulin in tetrads showing normal or abnormal configurations at 37°C. White, DAPI; green, α-tubulin. Frequencies represent the average rates of the corresponding phenotypes; n indicates the number of the analyzed plants or meiocytes; ***, $P < 0.001$; *, $P < 0.05$; ns, $P > 0.05$; scale bars, 10 µm.

DSB and CO formation in L*er* are largely resistant to heat

To assess the possible resilience of meiotic recombination towards heat in L*er*, we analyzed chromosomes by spreading and scored bivalent formation in Col and L*er* at 20°C and 37°C. At 20°C, five bivalents were present in diakinesis in both accessions (Fig. 2a and c). While bivalent formation in Col was completely impaired at 37°C, this was not the case in L*er* (Fig. 2a and c). To examine then the effect of heat on CO formation, immunolocalization of the type-I CO marker protein HEI10 was performed and the number of HEI10 foci on chromosomes in diakinesis was quantified. At 20°C, as previously reported, Col showed a higher number of HEI10 foci than L*er* with 11.0 foci versus 9.4, respectively (Fig. 2b and d) (Ziolkowski *et al.*, 2017). At 37°C, no HEI10 foci were detected in Col whereas L*er* showed an average of 10.5 HEI10 foci per meiocyte, being not significantly different from the number at 20°C (Fig. 2b and d). Moreover, all analyzed anaphase I meiocytes in heat-stressed Col showed mis-segregation of homologs while only 41.5% unequal homolog segregation occurred in L*er* under heat stress (Fig. 2e and f). Based on these data, we conclude that heat stress does not reduce CO formation in L*er*. Since heat stress has earlier been found to partially suppress CO formation by reducing DNA double-strand break (DSB) formation (Ning *et al.*, 2021), we next analyzed the localization of the DSB repair recombinases RAD51 and DMC1, two widely used DSB markers (Kurzbauer *et al.*, 2012; Kurzbauer *et al.*, 2021). Consistent with previous reports, both the numbers of RAD51 and DMC1 foci on zygotene chromosomes in Col were significantly reduced after heat treatment (Fig. 2g-j) (Ning *et al.*, 2021; Zhao *et al.*, 2023). In L*er*, however, the focus numbers of both proteins were not significantly altered by heat (Fig. 2g-j), suggesting that heat stress does not reduce DSB formation in L*er*.

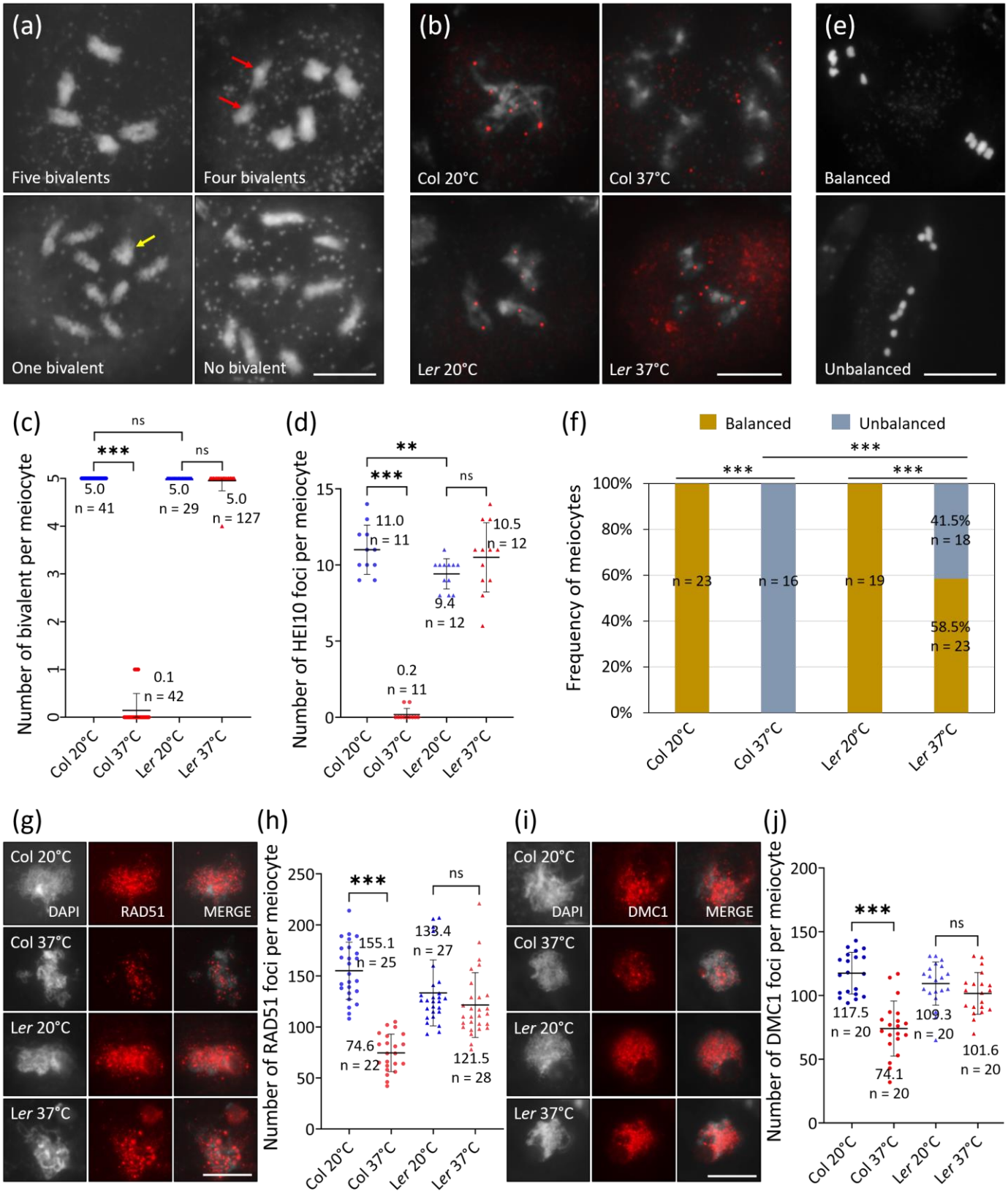

Figure 2. Heat stress does not reduce CO and DSB formation in L*er*. (a) Representative images of diakinesis meiocytes showing five, four, one or no bivalents. The red and yellow arrows indicate univalents and bivalent, respectively. (b) Immunolocalization of HEI10 in diakinesis meiocytes of Col and L*er* at 20°C and 37°C. (c and d) Graphs showing the average numbers of bivalent (c) and HEI10

233 foci (d) per meiocyte in Col and L*er* at 20°C and 37°C. Stars indicate significance levels based on unpaired *t* tests. (e) Representative
234 images of anaphase I meiocytes showing balanced and unequal homolog separation. (f) Graph showing the fraction of anaphase
235 I meiocytes with equal or unequal homolog separation in Col and L*er* at 20°C and 37°C. Stars provide significance levels based on
236 χ^2-tests. (g and i) Immunolocalization of RAD51 (g) and DMC1 (i) on zygotene chromosomes of Col and L*er* at 20°C and 37°C. (h
237 and j) Graphs showing the average numbers of RAD51 (h) and DMC1 (j) foci per meiocyte in Col and L*er* at 20°C and 37°C. Stars
238 indicate significance levels based on unpaired *t* tests; frequencies indicate the average number or fraction of the corresponding
239 phenotypes; n indicates the number of the analyzed cells; ***, $P < 0.001$; **, $P < 0.01$; ns, $P > 0.05$; scale bars, 10 µm.
240
241 **Homolog synapsis in L*er* is more tolerant to heat stress than in Col**
242
243 Disrupted homolog pairing is the main cause of impaired CO formation in Col under heat stress (Ning *et al.*, 2021).
244 Therefore, we compared heat tolerance of homolog pairing in Col and L*er*. We classified pachytene meiocytes into
245 three types based on juxtaposition status of homologs: full-pairing, which indicates meiocytes exhibiting fully
246 juxtaposed homologs (Fig. 3a, b and e); partial-pairing, which indicates meiocytes showing both juxtaposed and
247 unpaired regions between homologs (Fig. 3f-i); and no pairing that represents impairment of homolog juxtaposition
248 (Fig. 3c and d). As previously reported, homolog pairing and synapsis in Col were fully impaired at 37°C (Fig. 3a, c and
249 j) (Ning *et al.*, 2021). In L*er*, however, 63.1% of meiocytes exhibited full pairing (Fig. 3e and j), and 35.4% of meiocytes
250 showed partial pairing (Fig. 3f-i, red arrows; j), with only 1.5% meiocytes displaying no pairing (Fig. 3d and j). Next, we
251 compared the impact of heat on chromosome morphology and the assembly of the chromosome axis and
252 synaptonemal complex (SC) by analyzing the localization of ASY4 and ZYP1 on zygotene and pachytene chromosomes,
253 respectively. At 20°C, ASY4 were loaded on the whole DAPI-stained chromosome regions showing a linear
254 configuration (Fig. 3k and l). Heat induced patchy ASY4 signals in both Col and L*er* (Fig. 3k), but the fraction of this
255 phenotype in Col was significantly higher than that in L*er* (Fig. 3l, $P < 0.001$). Immunolocalization of ZYP1 showed that
256 the SC assembly in Col was disrupted by heat, which, however, occurred normally or was only partially perturbed in
257 most pachytene meiocytes in L*er* (Fig. 3m-s, and t, ~95.6%). These data indicate that homolog pairing and synapsis in
258 L*er* are less impacted by heat than in Col.
259

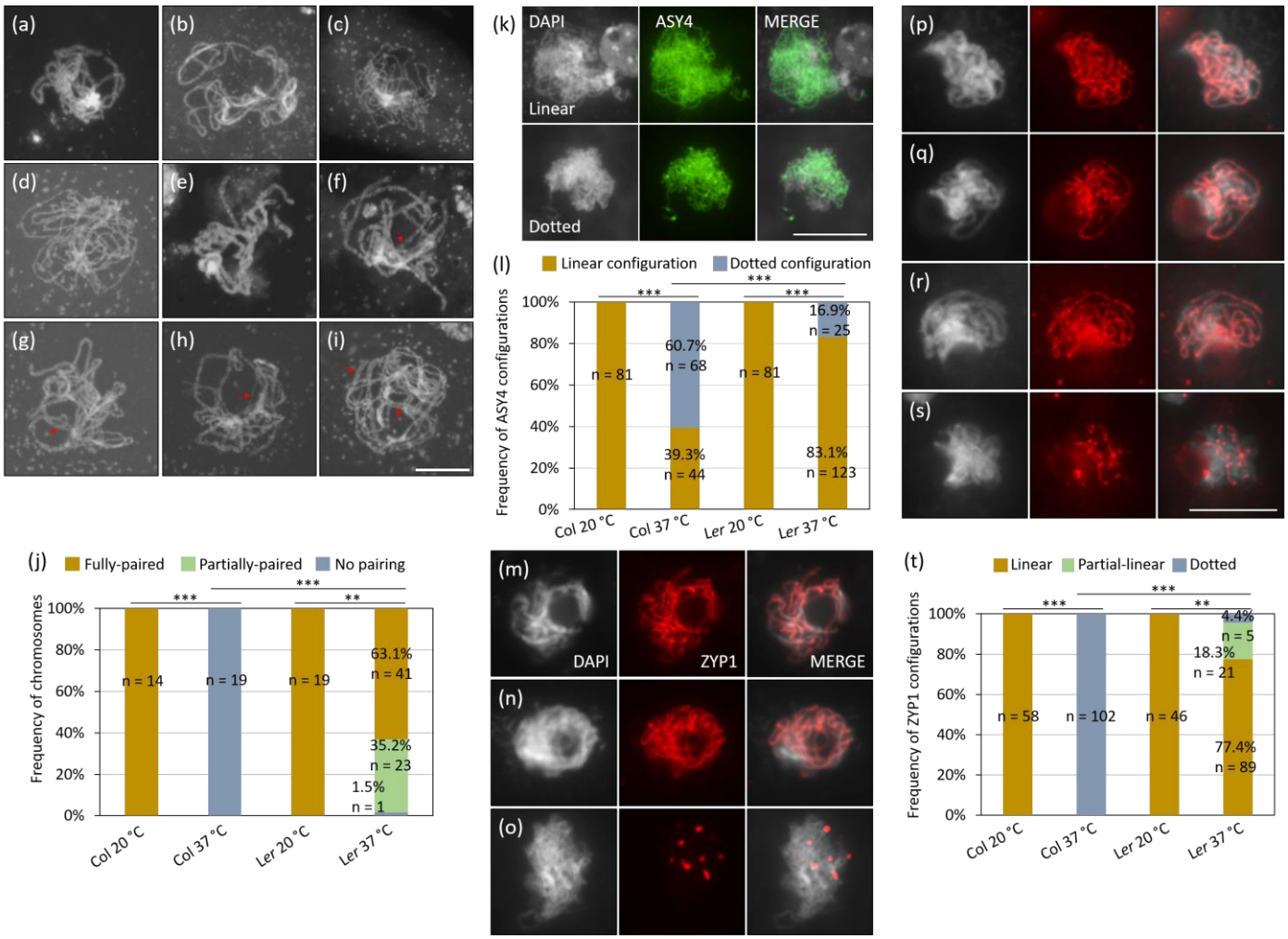

Figure 3. Homolog pairing and synapsis in L*er* are less impacted by heat than those in Col. (a-i) Pachytene chromosomes in Col (a and c) and L*er* (b, d-i) at 20°C (a and b) and 37°C (c-i). The red arrows indicate unpaired chromosome regions. (j) Graph showing the rates of pairing status of pachytene chromosomes in Col and L*er* at 20°C and 37°C. Stars indicate significance levels based on χ^2-tests. (k) Representative images of immunolocalization of ASY4 on chromosomes showing linear or patchy configurations. White, DAPI; green, ASY4. (l) Graph showing the rates of ASY4 configurations in Col and L*er* at 20°C and 37°C. Stars indicate significance levels based on χ^2-tests. (m-s) Immunolocalization of ZYP1 on pachytene chromosomes in Col (m and o) or L*er* (n, p-s) at 20°C (m and n) and 37°C (o-s). White, DAPI; red, ZYP1. (t) Graph showing the rates of ZYP1 configurations on pachytene chromosomes in Col and L*er* at 20°C and 37°C. Stars indicate significance levels based on χ^2-tests; frequencies indicate the rates of the corresponding phenotypes; n indicates the number of the analyzed cells; ***, $P < 0.001$; **, $P < 0.01$; scale bars, 10 µm.

Col/L*er* hybrids exhibit similar heat tolerance of meiotic recombination as L*er*

One of the main developmental differences between Col and L*er* is floral architecture (Fig. S2), which, in Arabidopsis,

274 is regulated by the receptor-like protein kinase ERECTA (ER) that acts upstream of the mitogen-activated protein kinase
275 cascade module MKK4/5-MPK3/6 (Meng *et al.*, 2012; Cai *et al.*, 2017). In addition, ER potentially plays a role in varied
276 heat responses between Col and L*er* (Zhang *et al.*, 2017; Lyu *et al.*, 2020). We thus examined whether the distinct heat
277 tolerance of meiotic recombination between Col and L*er* is owing to a loss of *ER*. To this end, we analyzed bivalent
278 formation, homolog separation, DMC1 and ASY4 localization, pachytene chromosome morphology as well as the SC
279 assembly in Col plants defective for ER and/or MPK6. Both the single *er* and *mpk6* and the double *er mpk6* mutants
280 displayed the same heat tolerance of meiotic recombination as Col (Fig. 4d, f, h, j and n).
281
282 To further explore the impact of the general genetic background on heat tolerance of meiosis, we analyzed
283 chromosome behavior in heat-stressed Col/L*er* hybrids, which exhibited the same flower architecture as Col (Fig. S2).
284 These plants produced a lower level of abnormal tetrads (~31.0%) than Col (Fig. 4a and b; Fig. 1b; $P < 0.001$).
285 Interestingly, bivalent formation in Col/L*er* hybrids was not reduced under heat stress (Fig. 4c and d), supporting the
286 conclusion that heat tolerance of meiotic recombination in L*er* is not conferred by the flower architecture. In addition,
287 balanced homolog segregation at anaphase I in heat-stressed Col/L*er* hybrids occurred at a similar frequency as in L*er*
288 (Fig. 4e and f; Fig. 2f; $P > 0.05$). Moreover, at 37°C, zygotene chromosomes in Col/L*er* hybrids showed an average
289 number of DMC1 foci (~116.0) significantly higher than those observed for Col (~74.1; $P < 0.001$) and L*er* (~101.6; $P <$
290 0.05) (Fig. 4g and h; Fig. 2j). Analysis of pachytene chromosome configurations and ASY4 localization revealed no
291 significant difference in heat tolerance between Col/L*er* hybrids and L*er* (Fig. 4i-l; Fig. 3j and l; $P > 0.05$). Furthermore,
292 most pachytene meiocytes (~74.1%) in Col/L*er* hybrids displayed a partial linear localization pattern of ZYP1, the extent
293 of which was higher than that in L*er* (Fig. 4m and n; Fig. 3t; $P < 0.001$); and the meiocytes showing linear or patchy
294 ZYP1 localization occupied 1.8% and 24.1%, respectively (Fig. 4m and n). Overall, these findings revealed similar heat
295 tolerance of meiotic recombination in Col/L*er* hybrids and in L*er*.
296

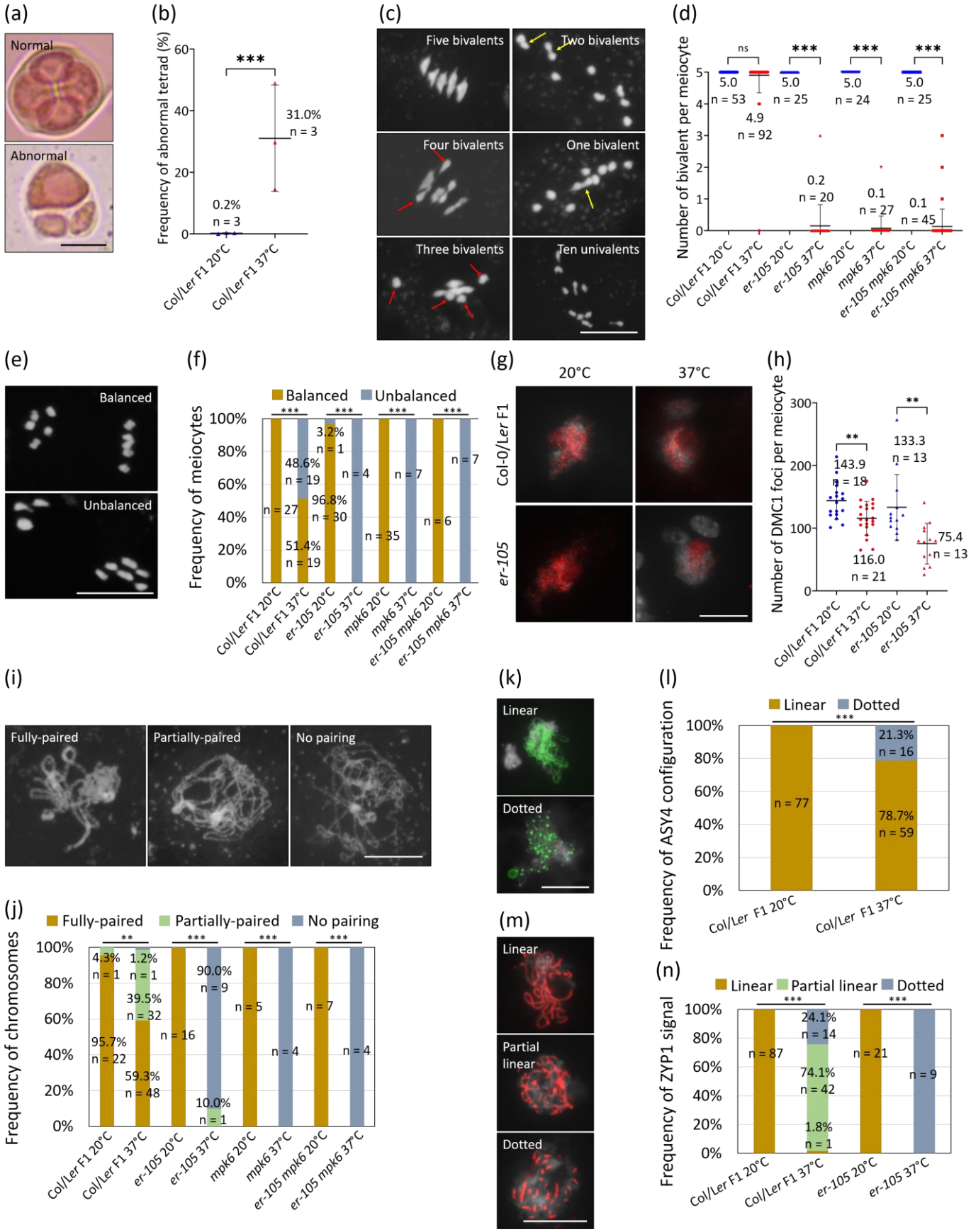

Figure 4. Col/*Ler* hybrids exhibit similar heat tolerance of meiotic recombination as *Ler*. (a) Representative images of normal and abnormal tetrads. (b) Graph showing the rates of abnormal tetrad in Col/*Ler* hybrids at 20°C and 37°C. (c) Representative images

300 of metaphase I chromosomes with different numbers of bivalents. The red and yellow arrows indicate univalents and bivalents,
301 respectively. (d) Graph showing the average numbers of bivalent per diakinesis and/or metaphase I meiocyte in Col/L*er* hybrids,
302 the single *er-105* and *mpk6*, and the double *er-105 mpk6* mutants at 20°C and 37°C. (e) Representative images of anaphase I
303 chromosomes showing balanced or unbalanced homolog separation. (f) Graph showing the frequencies of anaphase I meiocytes
304 with balanced or unbalanced homolog separation in Col/L*er* hybrids, the single *er-105* and *mpk6*, and the double *er-105 mpk6*
305 mutants at 20°C and 37°C. (g) Immunolocalization of DMC1 on zygotene chromosomes in Col/L*er* hybrids and *er-105* at 20°C and
306 37°C. White, DAPI; red, DMC1. (h) Graph showing the average numbers of DMC1 foci per meiocyte in Col/L*er* hybrids and *er-105*
307 at 20°C and 37°C. (i) Representative images of pachytene chromosomes showing full-pairing, partial-pairing, and no pairing. (j)
308 Graph showing the rates of pachytene meiocytes exhibiting full-pairing, partial-pairing and no pairing in Col/L*er* hybrids, the single
309 *er-105* and *mpk6* and the double *er-105 mpk6* mutants at 20°C and 37°C. (k) Representative images of immunolocalization of ASY4
310 on zygotene chromosomes showing different configurations. White, DAPI; green, ASY4. (l) Graph showing the frequencies of ASY4
311 configurations in Col/L*er* hybrids at 20°C and 37°C. (m) Representative images of immunolocalization of ZYP1 on pachytene
312 chromosomes showing different configurations. White, DAPI; red, ZYP1. (n) Graph showing the rates of ZYP1 configurations on
313 pachytene chromosomes in Col/L*er* hybrids and the single *er-105* mutant at 20°C and 37°C. In (b), (d) and (h), stars indicate
314 significance levels based on unpaired *t* tests; in (f), (j), (l) and (n), stars indicate significance levels based on χ^2-tests; ***, $P < 0.001$;
315 **, $P < 0.01$; ns, $P > 0.05$; numbers or frequencies indicate the quantities or fractions of the corresponding phenotypes; n indicates
316 the number of the analyzed individuals or cells. Scale bars, 10 µm.
317
318 **Heat tolerance of pairing and CO formation is largely lost in the progeny of Col/L*er* hybrids**
319
320 To further analyze the genetic underpinnings of heat tolerance of meiotic recombination, we examined homolog
321 pairing, synapsis and bivalent formation in the progeny of Col/L*er* hybrids under heat stress. Unexpectedly, in a
322 population of 1213 pachytene meiocytes from 132 Col/L*er* F2 individuals, only 11.1% of meiocytes showed full-pairing
323 of homologs. Partial-pairing and no pairing of homologs occurred 36.7% and 52.2%, respectively (Fig. 5a and b).
324 Furthermore, only 19.8% of analyzed meiocytes (n = 3391) had five bivalents whereas 45.8% of meiocytes showed ten
325 univalents, with the remaining 35% having either four, three, two or one bivalents occurring at roughly similar levels
326 (Fig. 5a and c). Accordingly, 48.4% of F2 individuals (n = 155) showed an average of at most one bivalent per meiocyte,
327 while 18.7% of F2 individuals showed an average of more than four bivalents per meiocyte (Fig. 5d). These data
328 indicated that, in the context of bivalent formation, around half of the Col/L*er* F2 individuals behaved like Col, while
329 only about 20.0% individuals displayed a L*er*-like resistance pattern under heat stress.

We analyzed the correlation of the impact of heat on pairing, bivalent formation, and homolog segregation in the heat-stressed Col/L*er* F2 population by performing Spearman's rank correlation tests using the frequencies of meiocytes showing different phenotypes (Fig. 5e). As expected, a strong and positive correlation was found between the numbers of bivalents and homolog pairing (Fig. 5e), with the presence of two, three or four bivalents per meiocyte being positively correlated with the partial-pairing phenotype (Fig. 5e). This correlation offered a proof that our assay system worked. Moreover, positive correlations were found between balanced homolog segregation and bivalent formation or successful pairing (Fig. 5e). Similar correlation patterns occurred in heat-stressed inbreds and F1 hybrids (Fig. S3). These findings suggested that DSB formation and/or early stages of DSB repair-mediated homolog pairing are possibly the primary targets of heat.

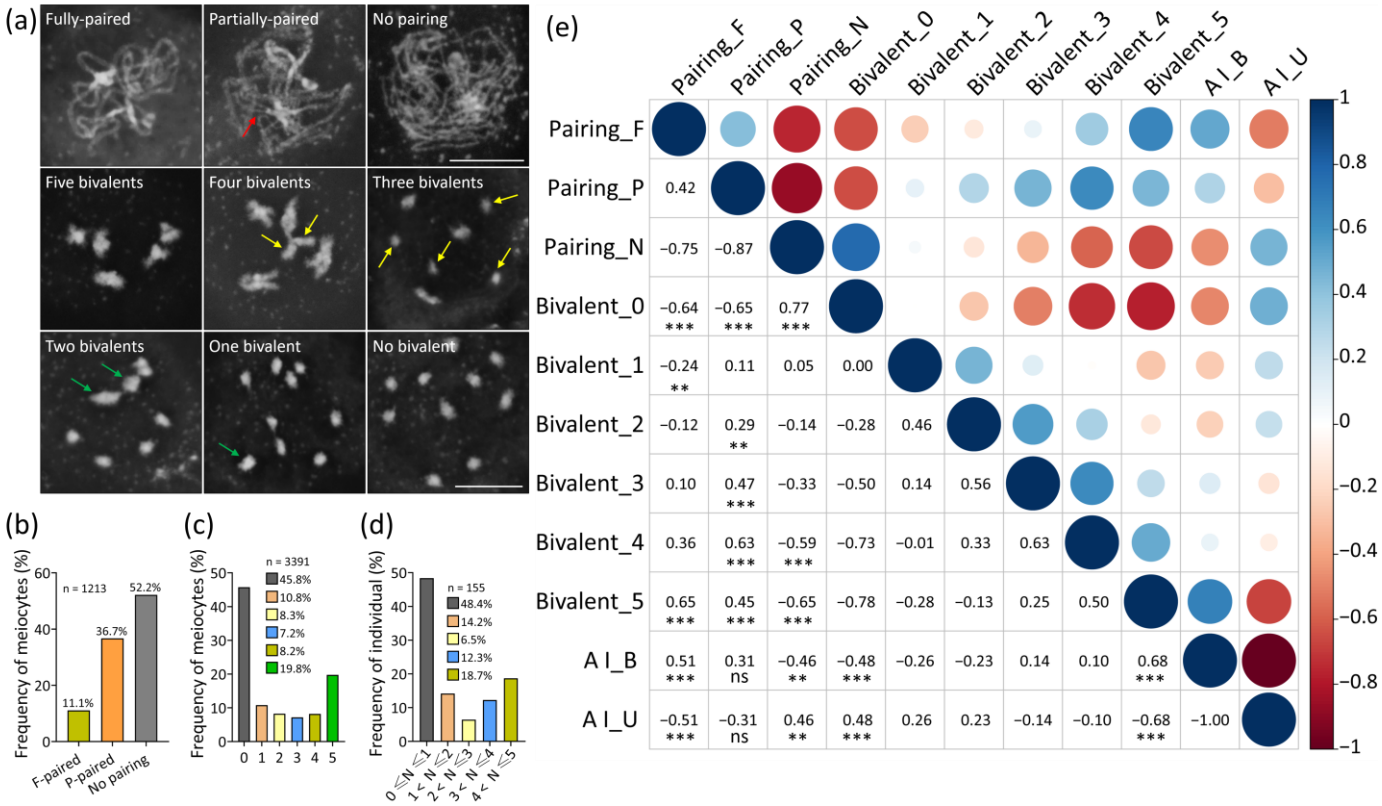

Figure 5. Chromosome pairing and bivalent formation in Col/L*er* F2 population under heat stress. (a) Representative images of chromosomes in pachytene and diakinesis showing different phenotypes of homolog pairing and bivalent formation in Col/L*er* F2 population under heat stress. The red, yellow and green arrows indicate unpaired or unsynapsed regions, univalents and bivalents, respectively. Scale bars, 10 µm. (b) Graph showing the fraction of pachytene meiocytes showing different pairing status in the heat-stressed Col/L*er* F2 population. (c) Graph showing the fraction of diakinesis meiocytes showing different numbers of bivalents

347 in the heat-stressed Col/L*er* F2 population. (d) Graph showing the fraction of individuals in heat-stressed Col/L*er* F2 population
348 showing different average numbers of bivalents. The frequencies indicate the rates of the corresponding phenotypes; n indicates
349 the numbers of meiocytes or individuals; N indicates the average numbers of bivalent per meiocyte. (e) Graph showing correlation
350 between pairing, average number of bivalents per meiocyte, and homolog segregation. Spearman correlation analysis was
351 performed; numbers indicate the correlation coefficients between the corresponding phenotypes; significance levels of
352 correlation were determined based on *t*-tests; ***, $P < 0.001$; **, $P < 0.01$; ns, $P > 0.05$; the significance levels in the cells without
353 indication of significance values were not calculated.
354
355 **Heat stress reveals different impacts on chromosome morphology in interkinesis between Col and L*er* inbreds and**
356 **their F2 offspring**
357
358 At the end of meiosis I, homologs temporally decondense at interkinesis and then recondense at metaphase II (Fig.
359 S4). We found that heat induced a less-condensed or non-condensed chromosome configuration in interkinesis, which
360 also varied between Col and L*er* (Fig. 6a and c). The chromosomes exhibiting either kind of alterations in condensation
361 showed a lower DAPI fluorescence intensity compared with the ones displaying normal condensation (Fig. 6a and b).
362 At 37°C, 25.0% Col plants produced meiocytes with a less-condensed chromosome configuration, while, this
363 phenotype was not observed in any analyzed L*er* plant individuals (Fig. 6c). Meanwhile, meiocytes showing a non-
364 condensed chromosome configuration were observed in both Col and L*er* under heat stress (Fig. 6c). Both kinds of
365 abnormalities were observed in Col/L*er* hybrids and F2 population (Fig. 6c). However, in the F2 offspring that displayed
366 altered chromosome morphology, the fraction of meiocytes displaying non-condensed chromosomes was similar to
367 that in Col but higher than those in L*er* and Col/L*er* hybrids (Fig. 6d), while the fraction of meiocytes exhibiting the
368 less-condensed phenotype was higher than those in inbreds and hybrids (Fig. 6e).
369
370 Interestingly, positive correlations were found between the less-condensed phenotype and impaired pairing or
371 formation of only a single bivalent per meiocyte (Fig. 6f and g). In addition, normal morphology of interkinesis
372 chromosomes was highly correlated with the presence of five bivalents per meiocyte (Fig. 6g). The non-condensed
373 phenotype was positively associated with compromised pairing and reduced bivalent formation (Fig. 6f and g). Taken
374 together, these findings implied that the loci controlling heat tolerance of homolog pairing and/or CO formation may
375 have a potential role in regulating chromosome morphology in interkinesis under heat stress.
376

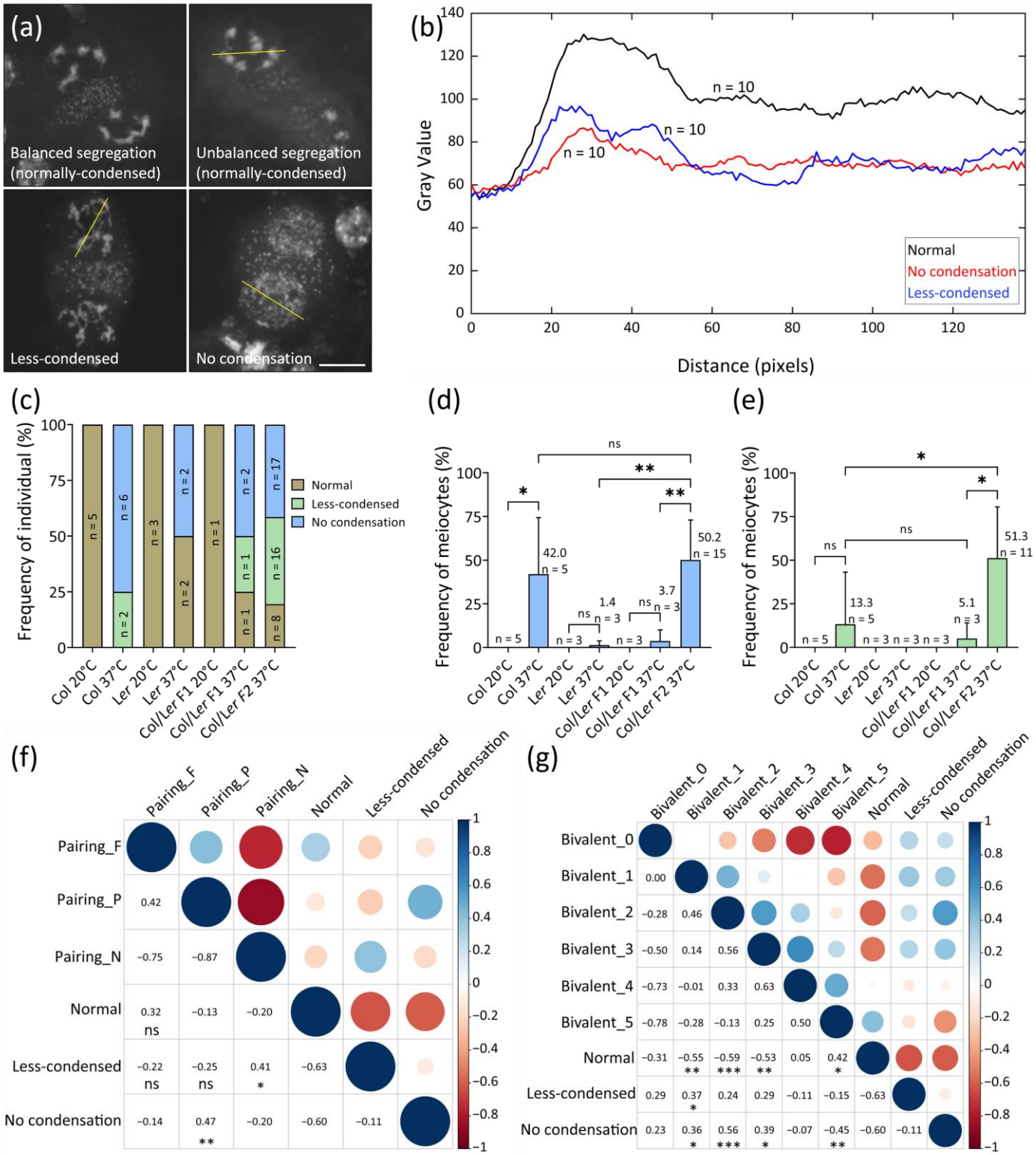

Figure 6. The impact of heat on chromosome morphology in interkinesis. (a) Representative images of different chromosome morphologies in interkinesis. Scale bar, 10 µm. (b) Average pixel intensity quantified in interkinesis meiocytes showing either kind of chromosome configuration of a section going through the middle of chromosomes (yellow lines). (c) Graph showing the rates of individuals with less-condensed or non-condensed phenotypes in Col, L*er*, Col/L*er* hybrids and Col/L*er* F2 at 20°C or 37°C. n

382 indicates the numbers of plant individuals. (d and e) Graphs showing the rates of meiocytes showing non-condensed (d) or less-
383 condensed (e) phenotypes in Col, L*er*, Col/L*er* hybrids and Col/L*er* F2 at 20°C or 37°C. Stars indicate significance levels based on
384 unpaired *t* tests; n indicates the numbers of plant individuals; frequencies indicate the rates of the corresponding phenotypes. (f)
385 and (g) Graphs showing the correlation between pairing (f) and average number of bivalents per meiocyte (g) with the less-
386 condensed or non-condensed phenotypes. Spearman correlation analysis was performed; numbers indicate the correlation
387 coefficients between the corresponding phenotypes; stars indicate significance levels based on unpaired *t* tests; ***, $P < 0.001$;
388 **, $P < 0.01$; *, $P < 0.05$; ns, $P > 0.05$; the significance levels in the cells without indication of significance values were not calculated.
389

390 **Heat stress induces high levels of chromosome instabilities in the Col/L*er* F2 population**

391

392 Heat did not significantly increase the fraction of individuals exhibiting premature segregation of sister chromatids in
393 Col and L*er* (Fig. 7a-d). In the Col/L*er* F2 population, however, 56.7% of individuals (n = 164) showed ectopic
394 segregation of sister chromatids from diakinesis to metaphase II (Fig. 7b and c), suggesting that sister-chromatid
395 cohesion was perturbed. In these defect-harboring F2 plants, the fraction of meiocytes showing untimely segregation
396 of sister chromatids was significantly higher than in parental genotypes (Fig. 7d). While we did not observe obvious
397 defects in chromosome integrity in Col and L*er* under heat stress, 27.0% of individuals (n = 126) in the heat-stressed
398 Col/L*er* F2 population produced chromosome fragments at metaphase I, anaphase I or metaphase II (Fig. 7e-g),
399 suggesting that DSB repair was defective in those F2 individuals under heat stress. Moreover, the average number of
400 fragments per meiocyte in those F2 individuals was higher than in the inbreds and hybrids (Fig. 7g). These data
401 suggested that heat tolerance of chromosome stability maintenance is affected in the Col/L*er* F2 population.
402

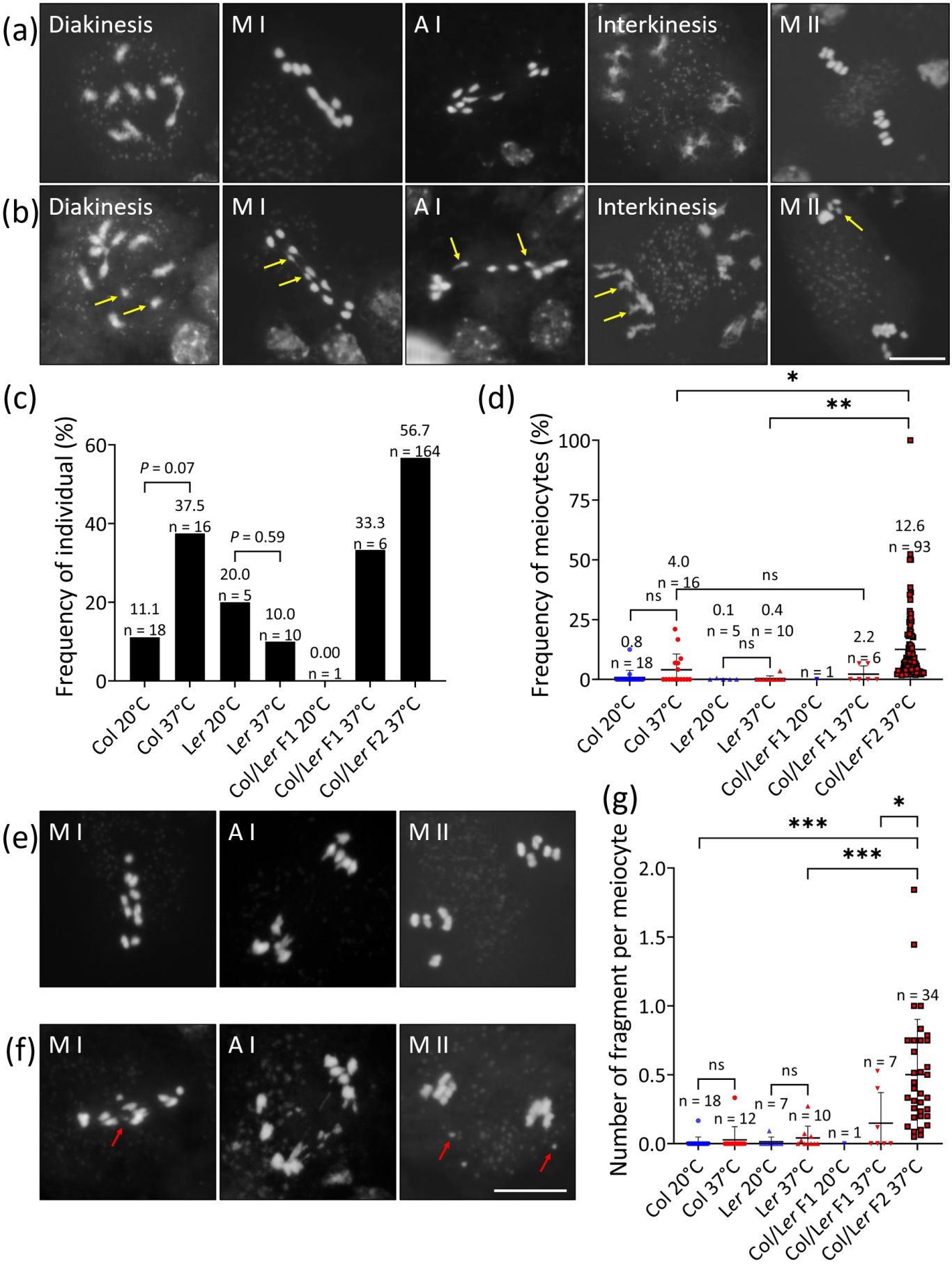
(a)
Diakinesis
M I
A I
Interkinesis
M II
(b)
Diakinesis
M I
A I
Interkinesis
M II
(c)
Frequency of individual (%)
60
40
20
0
P = 0.07
P = 0.59
11.1
n = 18
37.5
n = 16
20.0
n = 5
10.0
n = 10
0.00
n = 1
33.3
n = 6
56.7
n = 164
Col 20°C
Col 37°C
Ler 20°C
Ler 37°C
Col/Ler F1 20°C
Col/Ler F1 37°C
Col/Ler F2 37°C
(d)
Frequency of meiocytes (%)
100
75
50
25
0
*
**
ns
ns
ns
0.8
n = 18
4.0
n = 16
0.1
n = 5
0.4
n = 10
n = 1
2.2
n = 6
12.6
n = 93
Col 20°C
Col 37°C
Ler 20°C
Ler 37°C
Col/Ler F1 20°C
Col/Ler F1 37°C
Col/Ler F2 37°C
(e)
M I
A I
M II
(f)
M I
A I
M II
(g)
Number of fragment per meiocyte
2.0
1.5
1.0
0.5
0.0
***
***
*
ns
ns
n = 18
n = 12
n = 7
n = 10
n = 1
n = 7
n = 34
Col 20°C
Col 37°C
Ler 20°C
Ler 37°C
Col/Ler F1 20°C
Col/Ler F1 37°C
Col/Ler F2 37°C

404 Figure 7. The Col/L*er* F2 population shows a higher level of chromosome instability under heat stress. (a) and (b) Representative
405 images of diakinesis, metaphase I, anaphase I, interkinesis and metaphase II meiocytes showing normal (a) or pre-mature
406 segregation of sister chromatids (b) under heat stress. The yellow arrows indicate separated sister chromatids. (c) Graph showing
407 the rates of individuals that show abnormal segregation of sister chromatids in Col, L*er*, Col/L*er* hybrids and Col/L*er* F2 at 20°C or
408 37°C. The indicated significance levels were determined based on χ^2-tests. (d) Graph showing the rates of meiocytes exhibiting
409 premature separation of sister chromatids in Col, L*er*, Col/L*er* hybrids and Col/L*er* F2 at 20°C or 37°C. (e and f) Representative
410 images of metaphase I, anaphase I and metaphase II chromosomes with normal (e) or interfered integrity (f) under heat stress.
411 The red arrows indicate chromosome fragments. (g) Graph showing the average numbers of chromosome fragment per meiocyte
412 in Col, L*er*, Col/L*er* hybrids and Col/L*er* F2 at 20°C or 37°C. Stars indicate significance levels based on unpaired *t* tests; frequencies
413 indicate the rates of the corresponding phenotypes; n indicates the number of individuals; ***, $P < 0.001$; **, $P < 0.01$; *, $P < 0.05$;
414 ns, $P > 0.05$; scale bars, 10 µm.
415
416 **Homolog pairing and synapsis facilitate timely sister-chromatids separation under heat stress**
417
418 We then related homolog pairing and bivalent formation with the phenotype of premature sister-chromatids
419 separation in our heat-stressed Col/L*er* F2 population. A positive but weak correlation was detected between the
420 fraction of meiocytes showing cohesion defect with the fraction of meiocytes showing partial pairing, or the diakinesis
421 meiocytes producing an average of one bivalent (Fig. 8a and b). Notably, among the meiocytes showing ectopic sister-
422 chromatid separation, the meiocytes in metaphase I, anaphase I or metaphase II stages occupied 8.7%, 35.8% and
423 59.0%, respectively (Fig. 8c). This implied that heat stress primarily destabilizes centromeric cohesion in late or after
424 meiosis I. Moreover, we found a strong and positive correlation between the fraction of meiocytes exhibiting
425 chromosome fragmentations with meiocytes in pachytene undergoing normal homolog pairing (Fig. 8d) and with
426 meiocytes in diakinesis producing five bivalents (Fig. 8e).
427
428 To further investigate the impact of homolog pairing and/or synapsis and CO formation on sister-chromatids cohesion
429 under heat stress, we analyzed a *spo11-1* mutant (Col background), in which DSB formation is largely abolished and
430 homolog pairing and recombination are impaired (Xue *et al.*, 2018). Untimely separation of sister chromatids was
431 observed in *spo11-1* at both temperatures, but there was no significant difference (Fig. 8f-h, $P > 0.05$). Next, we
432 analyzed the *dmc1* (Col background), in which DSBs are formed but homolog pairing and CO formation do not occur
433 (Sanchez-Moran *et al.*, 2007), and the double *zyp1a*/*b* mutant (Col background), in which homolog pairing occurs but

434 synapsis is impaired (Capilla-Pérez *et al.*, 2021; France *et al.*, 2021; Yang *et al.*, 2022). Both *dmc1* and *zyp1a*/*b* exhibited
435 premature sister-chromatids segregation at 20°C, and, the fraction of meiocytes showing the cohesion defect in both
436 mutants were significantly increased under heat stress (Fig. 8f-h; $P < 0.01$ for *dmc1* and $P < 0.001$ for *zyp1a*/*b*).
437 Interestingly, the defect-harboring meiocytes in *dmc1* occurred by 66.7% at and/or prior to anaphase I, while, in
438 *zyp1a*/*b*, the irregularity was found by 79.2% at metaphase II (Fig. 8i). These findings implied that DMC1- and ZYP1-
439 dependent homolog pairing and/or synapsis play a role in facilitating timely separation of sister chromatids under heat
440 stress, yet possibly via different mechanisms. To address if the distinct distribution of differently-staged meiocytes
441 showing ectopic sister-chromatids separation between *dmc1* and *zyp1a*/*b* was owing to the difference in CO formation,
442 we examined a *msh4* mutant (Col background), which undergoes normal homolog synapsis but loses approximately
443 85% COs (Higgins *et al.*, 2004). No significant difference in the rates of meiocytes with cohesion defect was detected
444 at 20°C and 37°C (Fig. 8h, $P > 0.05$).
445

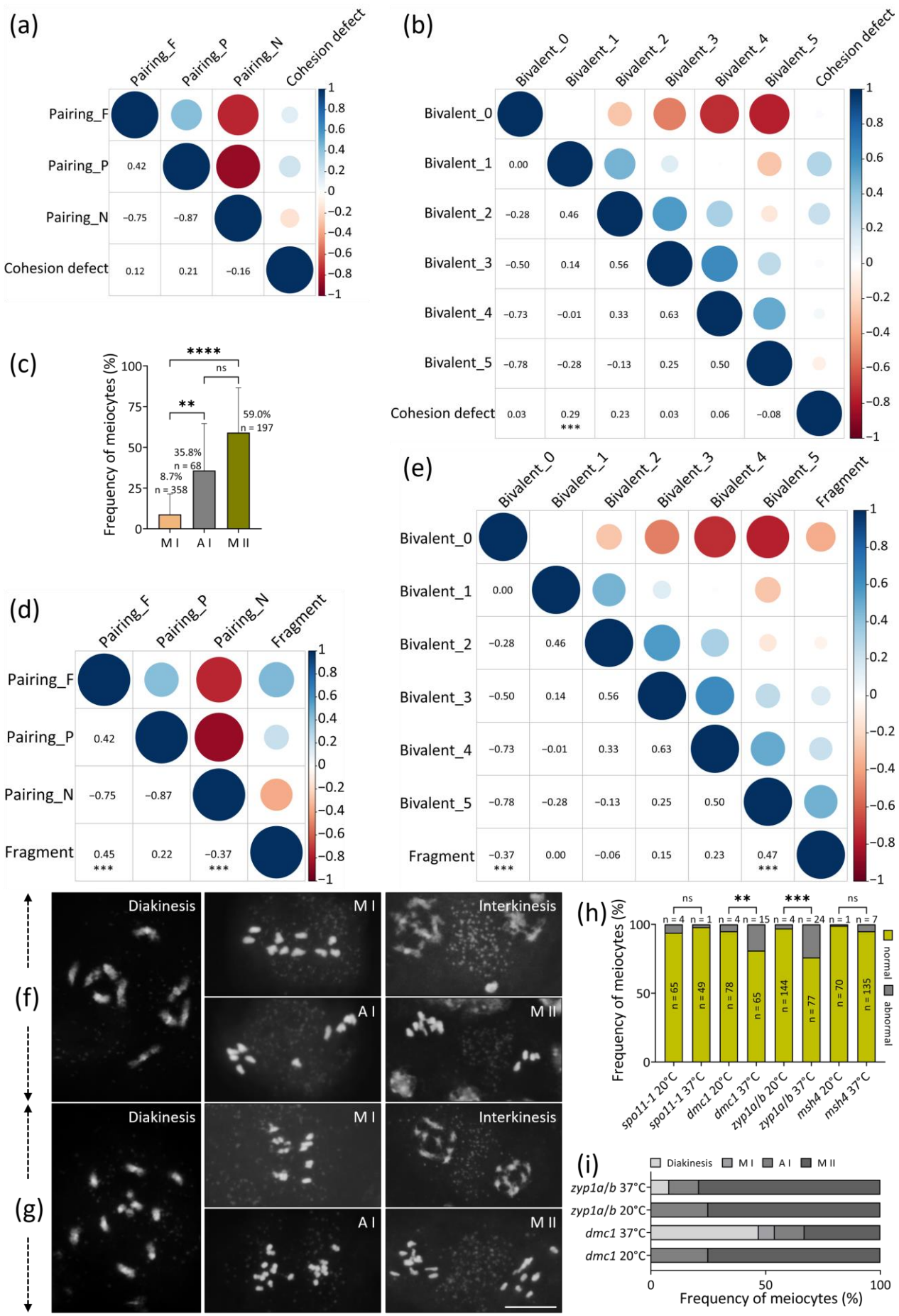
(a)
Pairing_F
Pairing_P
Pairing_N
Cohesion defect
0.42
−0.75
−0.87
0.12
0.21
−0.16
(b)
Bivalent_0
Bivalent_1
Bivalent_2
Bivalent_3
Bivalent_4
Bivalent_5
Cohesion defect
0.00
−0.28
0.46
−0.50
0.14
0.56
−0.73
−0.01
0.33
0.63
−0.78
−0.28
−0.13
0.25
0.50
0.03
0.29
***
0.23
0.03
0.06
−0.08
(c)
Frequency of meiocytes (%)
****
ns
**
8.7%
n = 358
35.8%
n = 68
59.0%
n = 197
M I
A I
M II
(d)
Pairing_F
Pairing_P
Pairing_N
Fragment
0.42
−0.75
−0.87
0.45
***
0.22
−0.37
***
(e)
Bivalent_0
Bivalent_1
Bivalent_2
Bivalent_3
Bivalent_4
Bivalent_5
Fragment
0.00
−0.28
0.46
−0.50
0.14
0.56
−0.73
−0.01
0.33
0.63
−0.78
−0.28
−0.13
0.25
0.50
−0.37
***
0.00
−0.06
0.15
0.23
0.47
***
(f)
Diakinesis
M I
Interkinesis
A I
M II
(g)
Diakinesis
M I
Interkinesis
A I
M II
(h)
Frequency of meiocytes (%)
ns
**
***
ns
n = 4
n = 1
n = 4
n = 15
n = 4
n = 24
n = 1
n = 7
n = 65
n = 49
n = 78
n = 65
n = 144
n = 77
n = 70
n = 135
normal
abnormal
spo11-1 20°C
spo11-1 37°C
dmc1 20°C
dmc1 37°C
zyp1a/b 20°C
zyp1a/b 37°C
msh4 20°C
msh4 37°C
(i)
Diakinesis
M I
A I
M II
zyp1a/b 37°C
zyp1a/b 20°C
dmc1 37°C
dmc1 20°C
Frequency of meiocytes (%)

446

447 Figure 8. Homolog pairing and synapsis facilitate timely sister-chromatids separation under heat stress. (a and b) Graphs showing
448 the correlation between the rates of meiocytes showing different pairing status (a) or bivalent formation (b) with the frequency
449 of meiocytes with cohesion defect in the Col/L*er* F2 population under heat stress. (c) Graph showing the rates of metaphase I,
450 anaphase I and metaphase II meiocytes with cohesion defect in the Col/L*er* F2 population under heat stress. (d and e) Graphs
451 showing the correlation between the frequencies of meiocytes showing different pairing status (d) or bivalent formation (e) with
452 the rate of meiocytes showing chromosome fragmentation in the Col/L*er* F2 population under heat stress. Spearman correlation
453 analysis was performed. Numbers indicate the correlation coefficients between the corresponding phenotypes; significance of
454 correlation was calculated using *t*-tests; the significance levels in the cells without indication of significance values were not
455 calculated. (f and g) Representative images of diakinesis, metaphase I, anaphase I, interkinesis and metaphase II meiocytes
456 showing normal (f) or untimely sister-chromatids separation (g). (h) Graph showing the rates of meiocytes with normal or untimely
457 sister-chromatids separation in *spo11-1*, *dmc1*, *zyp1a*/*b* and *msh4* at 20°C and 37°C. (i) Graph showing the rates of different
458 meiosis-staged meiocytes exhibiting untimely sister-chromatids separation in *dmc1* and *zyp1a*/*b* at 20°C and 37°C. For (c) and (h),
459 χ^2-tests were performed; frequencies indicate the rates of the corresponding phenotypes; n indicates the number of analyzed
460 cells; ***, $P < 0.001$; **, $P < 0.01$; ns, $P > 0.05$; scale bar, 10 µm.
461
462 **Chromosome integrity in both Col and L*er* under heat stress relies on functional ATM**
463
464 We previously reported that ATM-controlled DSB repair is required for maintenance of meiotic chromosome integrity
465 in Col under heat stress (Zhao *et al.*, 2023). Thus, we decided to examine whether the role of ATM in protecting
466 chromosome stability under heat stress varies between Col and L*er*. To this end, we took advantage of an *atm* mutant
467 allele, *atm-5*, which is in L*er* background and shows defects in DSB repair (Yao *et al.*, 2020). We found that, as the case
468 in *atm-2*, an allele in Col background (Zhao *et al.*, 2023), chromosome fragments in *atm-5* was significantly increased
469 after heat treatment (Fig. 9a and b; $P < 0.0001$). A bi-allelic *atm* mutant $ATM^{atm\text{-}2/atm\text{-}5}$, which harbored the *atm-2* and
470 *atm-5* alleles on either homolog, was generated, and behaved similarly as *atm-2* and *atm-5* under heat stress (Fig. 9c
471 and d). We also examined the impact of heat on homolog pairing in *atm-5*. At 20°C, most pachytene meiocytes showed
472 normal pairing and synapsis of homologs, and 16.9% of meiocytes showed a partial pairing phenotype (Fig. 9e and g).
473 At 37°C, most pachytene meiocytes in *atm-5* showed a partial pairing phenotype, with only 3.9% cells showing an
474 impaired homolog pairing (Fig. 9e and g), similar to the case in heat-stressed L*er* (Fig. 3j). Immunolocalization revealed
475 an increased level of patchy ZYP1 configuration in *atm-5* compared with that in L*er* (Fig. 9f and h; Fig. 3t), which was
476 likely caused by the disrupted chromosome integrity due to ATM dysfunction (Zhao *et al.*, 2023). Similar alterations in

homolog pairing and SC formation were observed in *ATM*$^{atm\text{-}2/atm\text{-}5}$ at either temperature (Fig. 9i-l). These data suggest that there is no accession-specific difference in dependency of ATM-mediated DSB repair for meiotic chromosome integrity under heat stress.

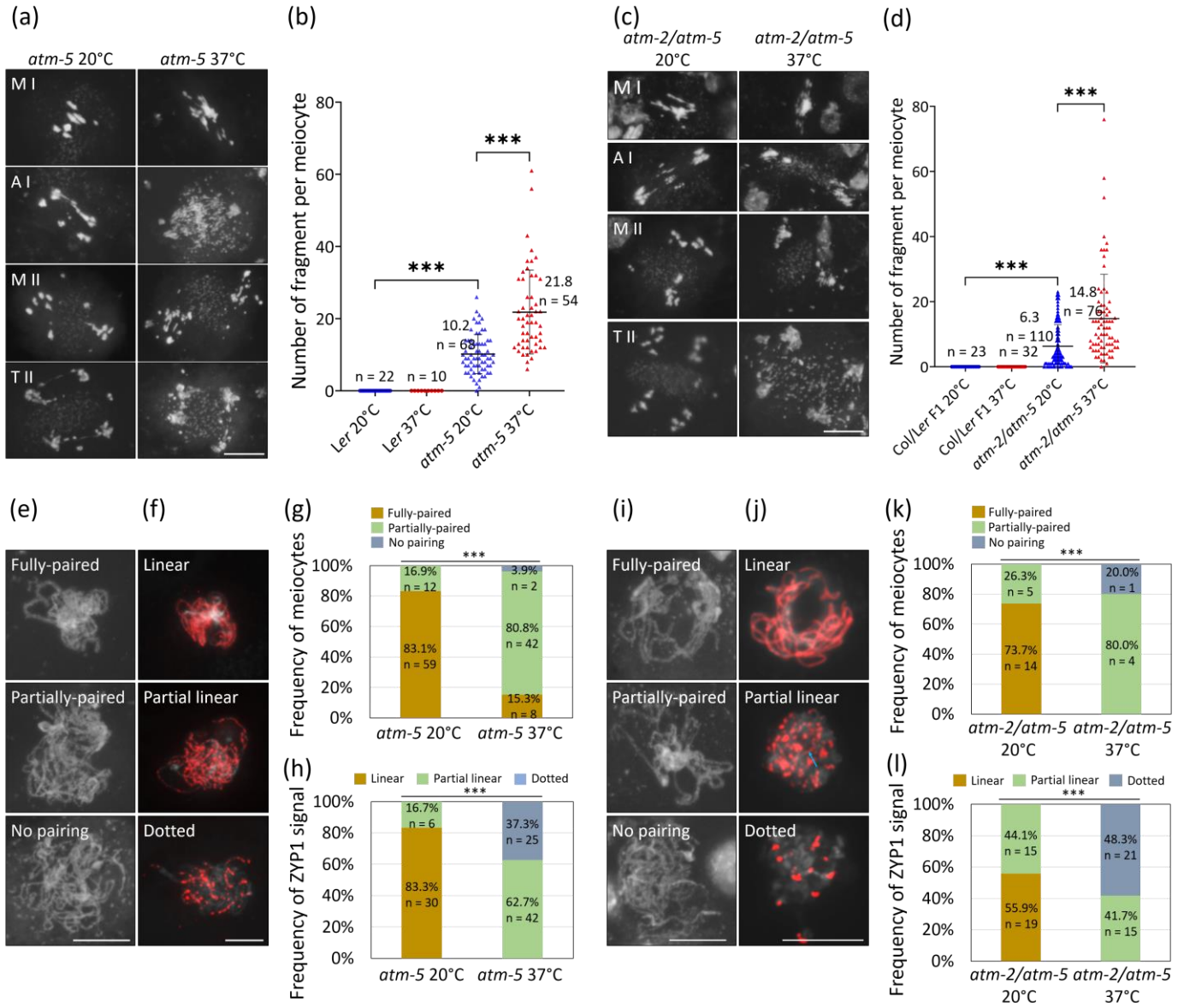

Figure 9. Chromosome integrity under heat stress in both Col and L*er* relies on ATM. (a and c), Metaphase I, anaphase I, metaphase II and telophase II chromosomes in *atm-5* (a) and *ATM*$^{atm\text{-}2/atm\text{-}5}$ (c) at 20°C and 37°C. (b and d), Graphs showing the average number of chromosome fragment in *atm-5* (b) and *ATM*$^{atm\text{-}2/atm\text{-}5}$ (d) at 20°C and 37°C. Significance levels are shown based on unpaired *t* tests. (e and i), Representative images of pachytene chromosomes showing fully-paired, partially-paired, or no pairing in *atm-5* (e) and *ATM*$^{atm\text{-}2/atm\text{-}5}$ (i) at 20°C and 37°C. (f and j), Representative images of immunolocalization of ZYP1 on pachytene chromosomes showing linear, partial linear, or patchy phenotypes in *atm-5* (f) and *ATM*$^{atm\text{-}2/atm\text{-}5}$ (j) at 20°C and 37°C. The blue arrow indicates

488 linear ZYP1 signals. (g and k), Graphs showing the rates of different pairing status of pachytene chromosomes in *atm-5* (g) and
489 *ATM*$^{atm-2/atm-5}$ (k) at 20°C and 37°C. Significance levels are shown based on χ^2-tests. (h and l), Graphs showing the rates of different
490 ZYP1 configurations on pachytene chromosomes in *atm-5* (h) and *ATM*$^{atm-2/atm-5}$ (l) at 20°C and 37°C. Significance levels are shown
491 based on χ^2-tests; frequencies or numbers indicate the rate or quantity of the corresponding phenotypes; n indicates the number
492 of analyzed cells; ***, $P < 0.001$; scale bars, 10 µm.
493
494 **Discussion**
495
496 Our previous study demonstrated that heat stress reduces DSB formation and disrupts pairing as well as synapsis of
497 homologs in Col (Ning *et al.*, 2021; Fu *et al.*, 2022). In this study, we report that Col and L*er* have a striking difference
498 in heat tolerance of meiotic recombination. Specifically, heat stress does not impair SC formation and does not reduce
499 the numbers of RAD51 or DMC1 foci in L*er* (Fig. 2 and 3). Based on our previous studies, the distinct heat tolerance of
500 DSB formation between Col and L*er* is likely due to a difference in the activity and/or localization of the recombination
501 proteins, and not in transcription levels (Ning *et al.*, 2021; Zhao *et al.*, 2023). Since the number of bivalents is strongly
502 correlated with homolog pairing status (Fig. 5), it is likely that heat suppresses meiotic recombination predominantly
503 by interfering with DSB formation and/or the RAD51- and DMC1-mediated homolog pairing. In support, DMC1 has
504 been found to play a role in maintaining CO formation at high temperature in wheat (Draeger *et al.*, 2019; Draeger *et*
505 *al.*, 2023). Nevertheless, since there is still a low level of DSBs in heat-stressed Col (Fig. 2), and some meiocytes in L*er*
506 display compromised homolog pairing under heat stress (Fig. 3), we propose that heat can also directly attenuate
507 homolog pairing apart from reducing DSB formation (Grelon *et al.*, 2001; Ning *et al.*, 2021; Fu *et al.*, 2022; Zhao *et al.*,
508 2023). Based on the analysis of Col/L*er* hybrids, we conclude that the heat tolerance of meiotic recombination in L*er*
509 is a dominant trait (Fig. 4). 10% ~ 20% of F2 offspring behaving as L*er* suggests that the dominance relies on the
510 presence of several alleles. While all alleles are present in Col/L*er* hybrids, the linkage of these alleles is broken in the
511 meiosis of these hybrids leading to a differentiated pattern of heat tolerance in the F2 population (Fig. 5).
512
513 Heat induces an increased fraction of interkinesis meiocytes displaying a non-condensed chromosome configuration
514 in Col, which does not occur in L*er* and the Col/L*er* F1 hybrids, but occurs again, and, at the same level, in the F2
515 population (Fig. 6d). Meanwhile, heat increases the rate of interkinesis meiocytes exhibiting a less-condensed
516 phenotype in some F2 individuals but not in inbreds or hybrids, which suggests a higher heat sensitivity in F2 offspring
517 (Fig. 6e). The heat-induced abnormalities in interkinesis phenotypically mimic slowed meiosis progression or a failure

518 of entering into meiosis II, which implies that meiosis progression and/or cell cycle transition may be perturbed
519 possibly due to alterations in expression and/or function of *TAM/CYCA1;2* (*TAM*) or *OMISSION OF SECOND DIVISION 1*
520 (*OSD1*), or other meiotic cell cycle regulators (Cromer *et al.*, 2012; Prusicki *et al.*, 2019; Ning *et al.*, 2021; Schindfessel
521 *et al.*, 2022). Furthermore, correlation analysis suggests that meiotic recombination or its related regulators may
522 impact meiotic cell cycle progression and/or chromosome morphology after anaphase I beyond its impact on prophase
523 I progression under heat stress (Fig. 6) (De Jaeger-Braet *et al.*, 2022).
524
525 Incorrect sister-chromatids separation in the F2 offspring (Fig. 7) implies that heat perturbs the function of the
526 cohesion complex. It has recently been reported that high temperatures reduce the amounts of CENH3 in Arabidopsis
527 (Crhak Khaitova *et al.*, 2024), which may lead to interfered centromere function and cohesion instability. Notably, we
528 found that most meiocytes showing cohesion defects are in anaphase I or metaphase II (Fig. 8), suggesting that heat
529 primarily perturbs centromeric cohesion during anaphase I and interkinesis. In Arabidopsis, SHUGOSHIN 1 (SGO1) and
530 PROTEIN PHOSPHATASE 2A (PP2A), and the Arabidopsis homolog of securin PATRONUS (PANS1) protect meiotic
531 centromeric cohesion at anaphase I and diakinesis, respectively (Cromer *et al.*, 2013; Zamariola *et al.*, 2014; Yuan *et*
532 *al.*, 2018; Cromer *et al.*, 2019). In addition, PP2A is co-expressed with genes involved in response to abiotic stresses
533 including heat in multiple developmental stages in Arabidopsis (Khan *et al.*, 2020). It is thus possible that heat stress
534 alters the expression and/or function of these cohesion regulators. In multiple species, bivalent formation is required
535 for correct orientation of sister kinetochores and thus balanced chromosome segregation in meiosis I (Hunt *et al.*,
536 1995; Rebollo & Arana, 1995; Khodjakov *et al.*, 1997; Chan & Cande, 1998; Yamamoto & Hiraoka, 2003; Xue *et al.*,
537 2019). Our correlation analysis suggests that homolog pairing and/or synapsis but possibly not chiasmata formation
538 may directly or indirectly impact timely sister-chromatids separation under heat stress (Fig. 8). However, heat-stressed
539 *spo11-1* does not show a higher level of defective sister-chromatids separation (Fig. 8), suggesting that the effect of
540 heat stress on homolog pairing-mediated cohesion stability may rely on DSB formation, and, the increased aneuploid
541 nuclei due to chromosome mis-segregation observed in heat-stressed *spo11-2* are not owing to premature sister-
542 chromatids separation (Crhak Khaitova *et al.*, 2024).
543
544 We observed an increase of chromosome fragments in some Col/L*er* F2 individuals but not in either inbreds or hybrids
545 under heat stress (Fig. 7), suggesting that DSB repair is perturbed in those fragment-harboring F2 plants. This
546 phenotype, together with the increased fraction of meiocytes showing premature sister-chromatid separation, imply
547 that transgressive effects become visible in the F2 population showing defects exceeding that observed in parents.

ATM-mediated DSB repair is required for meiotic chromosome integrity in both Col and L*er* under heat stress (Fig. 9) (Zhao *et al.*, 2023), dysfunction of which might be one of the mechanisms that underpin the heat-interfered chromosome integrity in those F2 individuals. The upstream factor and/or signaling pathway that regulates ATM expression or activity in DSB repair in response to heat stress require further investigation. Our data suggest that there is no accession-specific difference in the dependency of ATM-mediated DSB repair for maintenance of meiotic chromosome integrity under heat stress. Alternatively, ATM-mediated mechanism acts in an epistatic manner to protect meiotic chromosome stability under heat stress. Interestingly, the fragmentation phenotype is strongly and positively correlated with successful homolog pairing and bivalent formation (Fig. 8d and e). We speculate that these associations are possibly a subsequent effect of heat stress on DSB formation and repair, the heat tolerance of which are regulated via different pathways. Specifically, in the individuals that show normal homolog pairing and CO formation, DSB formation likely occurs normally, however, DSB repair may be perturbed, which consequently leads to lesions in chromosome integrity. On the contrary, the individuals with impaired homolog pairing and CO formation likely have a significantly reduced DSB formation, which compensates for the perturbation of DSB repair, and thus show relatively undisturbed chromosome integrity. Taken together, our study reveals that natural variation in multiple genomic loci controls heat tolerance of meiosis in Arabidopsis, with DSB formation and homolog pairing possibly being the predominant targets, which facilitate meiosis progression and genome stability after meiotic recombination at high temperatures.

Acknowledgement

The authors thank the National Natural Science Foundation of China (32000245), Hubei Provincial Natural Science Foundation of China (2024AFB695), the Fundamental Research Funds for the Central Universities of South-Central Minzu University (CZZ24011), Knowledge Innovation Program of Wuhan-Shuguang Project (2022020801020410) and general funds of University of Hamburg (to A.S.) for the financial support on this study. They thank Pingli Lu (Henan University) for sharing the *atm-5* mutants. They thank Chao Yang (HZAU) for providing the *zyp1a*/*b* mutant. They thank Yuan Qin (FAFU) for sharing the *er-105*, *mpk6* and the *er-105 mpk6* mutants.

Conflicts of interest

None declared.

578

579 **Data availability**

580

581 All data that support the conclusions drawn in our study are fully documented in this article and Supporting
582 Information (including Fig. S1–S4; Table S1).

583

584 **Author contributions**

585

586 J.Z. and H.F. performed most cytological experiments, genotyped plants, analyzed data, and edited manuscript; Z.W.,
587 Z.R., Z.W. and X.L. performed statistical analysis; M.Z., Y.L., X.C., W.P., Y.Z., X.G. and L.H. analyzed chromosome spreads;
588 C.W., A.S. and W.P. analyzed data and edited manuscript; B.L. conceived the project, designed experiments, analyzed
589 data, wrote, and edited the manuscript.

590

591 **Accession numbers**

592

593 Accession numbers of genes studied in this work are: *SPO11-1* (AT3G13170), *RAD51* (AT5G20850), *DMC1* (AT3G22880),
594 *ASY4* (AT2G33793), *ZYP1A* (AT1G22260), *ZYP1B* (AT1G22275), *HEI10* (AT1G53490), *ERECTA* (AT2G26330), *MPK6*
595 (AT2G43790), *ATM* (AT3G48190) and *MSH4* (AT4G17380).

596

597 **References**

598

599 **Ahmadli U, Kalidass M, Khaitova LC, Fuchs J, Cuacos M, Demidov D, Zuo S, Pecinkova J, Mascher M, Ingouff M, et al. 2023.** High
600 temperature increases centromere-mediated genome elimination frequency and enhances haploid induction in
601 Arabidopsis. *Plant Communications* **4**(3): 100507.

602 **Armstrong SJ, Caryl AP, Jones GH, Franklin FC. 2002.** Asy1, a protein required for meiotic chromosome synapsis, localizes to axis-
603 associated chromatin in Arabidopsis and Brassica. *Journal of Cell Science* **115**(Pt 18): 3645-3655.

604 **Armstrong SJ, Jones GH. 2003.** Meiotic cytology and chromosome behaviour in wild-type Arabidopsis thaliana. *Journal of*
605 *Experimental Botany* **54**(380): 1-10.

606 **Bomblies K, Higgins JD, Yant L. 2015.** Meiosis evolves: adaptation to external and internal environments. *New Phytologist* **208**(2):
607 306-323.

608 **Cai H, Zhao L, Wang L, Zhang M, Su Z, Cheng Y, Zhao H, Qin Y. 2017.** ERECTA signaling controls Arabidopsis inflorescence
609 architecture through chromatin-mediated activation of PRE1 expression. *New Phytologist* **214**(4): 1579-1596.

610 **Capilla-Pérez L, Durand S, Hurel A, Lian Q, Chambon A, Taochy C, Solier V, Grelon M, Mercier R. 2021.** The synaptonemal complex
611 imposes crossover interference and heterochiasmy in Arabidopsis. *Proc Natl Acad Sci U S A* **118**(12): e2023613118.

612 **Chambon A, West A, Vezon D, Horlow C, De Muyt A, Chelysheva L, Ronceret A, Darbyshire A, Osman K, Heckmann S, et al. 2018.**
613 Identification of ASYNAPTIC4, a component of the meiotic chromosome axis. *Plant Physiology* **178**(1): 233-246.
614 **Chan A, Cande WZ. 1998.** Maize meiotic spindles assemble around chromatin and do not require paired chromosomes. *Journal*
615 *of Cell Science* **111**(23): 3507-3515.
616 **Chelysheva L, Grandont L, Vrielynck N, Guin Sl, Mercier R, Grelon M. 2010.** An easy protocol for studying chromatin and
617 recombination protein dynamics during Arabidopsis thaliana meiosis: immunodetection of cohesins, histones and MLH1.
618 *Cytogenetic and Genome Research* **129**(1/3): 143-153.
619 **Chen H, He C, Wang C, Wang X, Ruan F, Yan J, Yin P, Wang Y, Yan S. 2021.** RAD51 supports DMC1 by inhibiting the SMC5/6 complex
620 during meiosis. *Plant Cell* **33**(8): 2869-2882.
621 **Chen Y, Dubois M, Vermeersch M, Inzé D, Vanhaeren H. 2021.** Distinct cellular strategies determine sensitivity to mild drought of
622 Arabidopsis natural accessions. *Plant Physiology* **186**(2): 1171-1185.
623 **Chen Y, Zhang Q, Teng Z, Liu H. 2021.** Centromeric transcription maintains centromeric cohesion in human cells. *Journal of Cell*
624 *Biology* **220**(7).
625 **Choi WG, Barker RJ, Kim SH, Swanson SJ, Gilroy S. 2019.** Variation in the transcriptome of different ecotypes of Arabidopsis
626 thaliana reveals signatures of oxidative stress in plant responses to spaceflight. *American Journal of Botany* **106**(1): 123-
627 136.
628 **Couteau F, Belzile F, Horlow C, Grandjean O, Vezon D, Doutriaux MP. 1999.** Random chromosome segregation without meiotic
629 arrest in both male and female meiocytes of a dmc1 mutant of Arabidopsis. *Plant Cell* **11**(9): 1623-1634.
630 **Crhak Khaitova L, Mikulkova P, Pecinkova J, Kalidass M, Heckmann S, Lermontova I, Riha K. 2024.** Heat stress impairs centromere
631 structure and segregation of meiotic chromosomes in Arabidopsis. *eLife* **12**.
632 **Cromer L, Heyman J, Touati S, Harashima H, Araou E, Girard C, Horlow C, Wassmann K, Schnittger A, De Veylder L, et al. 2012.**
633 OSD1 promotes meiotic progression via APC/C inhibition and forms a regulatory network with TDM and CYCA1;2/TAM.
634 *Plos Genetics* **8**(7): e1002865.
635 **Cromer L, Jolivet S, Horlow C, Chelysheva L, Heyman J, De Jaeger G, Koncz C, De Veylder L, Mercier R. 2013.** Centromeric cohesion
636 is protected twice at meiosis, by SHUGOSHINs at anaphase I and by PATRONUS at interkinesis. *Current Biology* **23**(21):
637 2090-2099.
638 **Cromer L, Jolivet S, Singh DK, Berthier F, De Winne N, De Jaeger G, Komaki S, Prusicki MA, Schnittger A, Guérois R, et al. 2019.**
639 Patronus is the elusive plant securin, preventing chromosome separation by antagonizing separase. *Proc Natl Acad Sci U*
640 *S A* **116**(32): 16018-16027.
641 **Da Ines O, Degroote F, Goubely C, Amiard S, Gallego ME, White CI. 2013.** Meiotic recombination in Arabidopsis is catalysed by
642 DMC1, with RAD51 playing a supporting role. *Plos Genetics* **9**(9): e1003787.
643 **De Jaeger-Braet J, Krause L, Buchholz A, Schnittger A. 2022.** Heat stress reveals a specialized variant of the pachytene checkpoint
644 in meiosis of Arabidopsis thaliana. *Plant Cell* **34**(1): 433-454.
645 **De Jaeger-Braet J, Schnittger A. 2024.** Heating up meiosis – chromosome recombination and segregation under high temperatures.
646 *Current Opinion in Plant Biology* **80**: 102548.
647 **De Storme N, Copenhaver GP, Geelen D. 2012.** Production of diploid male gametes in Arabidopsis by cold-induced destabilization
648 of postmeiotic radial microtubule arrays. *Plant Physiology* **160**(4): 1808-1826.
649 **De Storme N, Geelen D. 2020.** High temperatures alter cross-over distribution and induce male meiotic restitution in Arabidopsis
650 thaliana. *Communications Biology* **3**(1): 187.
651 **Draeger T, A CM, Alabdullah AK, Pendle A, Rey MD, Shaw P, Moore G. 2019.** Dmc1 is a candidate for temperature tolerance
652 during wheat meiosis. *Theoretical and Applied Genetics*.
653 **Draeger TN, Rey MD, Hayta S, Smedley M, Martin AC, Moore G. 2023.** DMC1 stabilizes crossovers at high and low temperatures
654 during wheat meiosis. *Frontiers in Plant Science* **14**: 1208285.
655 **Ferdous M, Higgins JD, Osman K, Lambing C, Roitinger E, Mechtler K, Armstrong SJ, Perry R, Pradillo M, Cuñado N, et al. 2012.**

656 Inter-homolog crossing-over and synapsis in Arabidopsis meiosis are dependent on the chromosome axis protein AtASY3.
657 *Plos Genetics* **8**(2): e1002507-e1002507.
658 **France MG, Enderle J, Röhrig S, Puchta H, Franklin FCH, Higgins JD. 2021.** ZYP1 is required for obligate cross-over formation and
659 cross-over interference in Arabidopsis. *Proc Natl Acad Sci U S A* **118**(14).
660 **Fu H, Zhao J, Ren Z, Yang K, Wang C, Zhang X, Elesawi IE, Zhang X, Xia J, Chen C, et al. 2022.** Interfered chromosome pairing at
661 high temperature promotes meiotic instability in autotetraploid Arabidopsis. *Plant Physiology* **188**(2): 1210-1228.
662 **Grelon M, Vezon D, Gendrot G, Pelletier G. 2001.** AtSPO11-1 is necessary for efficient meiotic recombination in plants. *Embo j*
663 **20**(3): 589-600.
664 **Higgins JD, Armstrong SJ, Franklin FCH, Jones GH. 2004.** The Arabidopsis MutS homolog AtMSH4 functions at an early step in
665 recombination: evidence for two classes of recombination in Arabidopsis. *Genes & Development* **18**(20): 2557-2570.
666 **Hunt P, LeMaire R, Embury P, Sheean L, Mroz K. 1995.** Analysis of chromosome behavior in intact mammalian oocytes: monitoring
667 the segregation of a univalent chromosome during female meiosis. *Hum Mol Genet* **4**(11): 2007-2012.
668 **Jin C, Sun L, Trinh HK, Danny G. 2023.** Heat stress promotes haploid formation during CENH3-mediated genome elimination in
669 Arabidopsis. *Plant Reproduction* **36**(2): 147-155.
670 **Jones GH, Franklin FC. 2006.** Meiotic crossing-over: obligation and interference. *Cell* **126**(2): 246-248.
671 **Khan ZH, Agarwal S, Rai A, Memaya MB, Mehrotra S, Mehrotra R. 2020.** Co-expression network analysis of protein phosphatase
672 2A (PP2A) genes with stress-responsive genes in Arabidopsis thaliana reveals 13 key regulators. *Scientific Reports* **10**(1):
673 21480.
674 **Khodjakov A, Cole RW, McEwen BF, Buttle KF, Rieder CL. 1997.** Chromosome fragments possessing only one kinetochore can
675 congress to the spindle equator. *Journal of Cell Biology* **136**(2): 229-240.
676 **Kurzbauer M-T, Janisiw MP, Paulin LF, Prusén Mota I, Tomanov K, Krsicka O, Haeseler Av, Schubert V, Schlögelhofer P. 2021.** ATM
677 controls meiotic DNA double-strand break formation and recombination and affects synaptonemal complex organization
678 in plants. *Plant Cell*.
679 **Kurzbauer MT, Uanschou C, Chen D, Schlogelhofer P. 2012.** The recombinases DMC1 and RAD51 are functionally and spatially
680 separated during meiosis in Arabidopsis. *Plant Cell* **24**(5): 2058-2070.
681 **Lambing C, Kuo PC, Tock AJ, Topp SD, Henderson IR. 2020.** ASY1 acts as a dosage-dependent antagonist of telomere-led
682 recombination and mediates crossover interference in Arabidopsis. *Proc Natl Acad Sci U S A* **117**(24): 13647-13658.
683 **Lambing C, Tock AJ, Topp SD, Choi K, Kuo PC, Zhao X, Osman K, Higgins JD, Franklin FCH, Henderson IR. 2020.** Interacting genomic
684 landscapes of REC8-cohesin, chromatin, and meiotic recombination in Arabidopsis. *Plant Cell* **32**(4): 1218-1239.
685 **Lardon R, Wijnker E, Keurentjes J, Geelen D. 2020.** The genetic framework of shoot regeneration in Arabidopsis comprises master
686 regulators and conditional fine-tuning factors. *Communications Biology* **3**(1): 549.
687 **Lasky JR, Des Marais DL, Lowry DB, Povolotskaya I, McKay JK, Richards JH, Keitt TH, Juenger TE. 2014.** Natural variation in abiotic
688 stress responsive gene expression and local adaptation to climate in Arabidopsis thaliana. *Molecular Biology and*
689 *Evolution* **31**(9): 2283-2296.
690 **Lei X, Ning Y, Eid Elesawi I, Yang K, Chen C, Wang C, Liu B. 2020.** Heat stress interferes with chromosome segregation and
691 cytokinesis during male meiosis in Arabidopsis thaliana. *Plant Signaling & Behavior* **15**(5): 1746985.
692 **Liu B, De Storme N, Geelen D. 2017.** Gibberellin induces diploid pollen formation by interfering with meiotic cytokinesis. *Plant*
693 *Physiology* **173**(1): 338-353.
694 **Liu B, De Storme N, Geelen D. 2018.** Cold-induced male meiotic restitution in Arabidopsis thaliana is not mediated by GA-DELLA
695 signaling. *Frontiers in Plant Science* **9**: 91.
696 **Liu B, Mo WJ, Zhang D, De Storme N, Geelen D. 2019.** Cold influences male reproductive development in plants: a hazard to
697 fertility, but a window for evolution. *Plant Cell Physiology* **60**(1): 7-18.
698 **Lloyd A, Morgan C, H. Franklin FC, Bomblies K. 2018.** Plasticity of meiotic recombination rates in response to temperature in
699 Arabidopsis. *Genetics* **208**(4): 1409-1420.

Lyu YS, Shao YJ, Yang ZT, Liu JX. 2020. Quantitative proteomic analysis of ER stress response reveals both common and specific features in two contrasting ecotypes of Arabidopsis thaliana. *Int J Mol Sci* **21**(24).

McKinley KL, Cheeseman IM. 2016. The molecular basis for centromere identity and function. *Nature Reviews Molecular Cell Biology* **17**(1): 16-29.

Meng X, Wang H, He Y, Liu Y, Walker JC, Torii KU, Zhang S. 2012. A MAPK cascade downstream of ERECTA receptor-like protein kinase regulates Arabidopsis inflorescence architecture by promoting localized cell proliferation. *Plant Cell* **24**(12): 4948-4960.

Modliszewski JL, Copenhaver GP. 2017. Meiotic recombination gets stressed out: CO frequency is plastic under pressure. *Current Opinion in Plant Biology* **36**: 95-102.

Modliszewski JL, Wang H, Albright AR, Lewis SM, Bennett AR, Huang J, Ma H, Wang Y, Copenhaver GP. 2018. Elevated temperature increases meiotic crossover frequency via the interfering (Type I) pathway in Arabidopsis thaliana. *Plos Genetics* **14**(5): e1007384.

Ning Y, Liu Q, Wang C, Qin E, Wu Z, Wang M, Yang K, Elesawi IE, Chen C, Liu H, et al. 2021. Heat stress interferes with formation of double-strand breaks and homolog synapsis. *Plant Physiology* **185**(4): 1783-1797.

Nore A, Juarez-Martinez AB, Clément J, Brun C, Diagouraga B, Laroussi H, Grey C, Bourbon HM, Kadlec J, Robert T, et al. 2022. TOPOVIBL-REC114 interaction regulates meiotic DNA double-strand breaks. *Nature Communications* **13**(1): 7048.

Onn I, Heidinger-Pauli JM, Guacci V, Unal E, Koshland DE. 2008. Sister chromatid cohesion: a simple concept with a complex reality. *Annu Rev Cell Dev Biol* **24**: 105-129.

Prusicki MA, Keizer EM, van Rosmalen RP, Komaki S, Seifert F, Müller K, Wijnker E, Fleck C, Schnittger A. 2019. Live cell imaging of meiosis in Arabidopsis thaliana. *eLife* **8**: e42834.

Rebollo E, Arana P. 1995. A comparative study of orientation at behavior of univalent in living grasshopper spermatocytes. *Chromosoma* **104**(1): 56-67.

Sanchez-Moran E, Santos JL, Jones GH, Franklin FC. 2007. ASY1 mediates AtDMC1-dependent interhomolog recombination during meiosis in Arabidopsis. *Genes & Development* **21**(17): 2220-2233.

Schiavon M, Zhang L, Abdel-Ghany SE, Pilon M, Malagoli M, Pilon-Smits EAH. 2007. Variation in copper tolerance in Arabidopsis thaliana accessions Columbia, Landsberg erecta and Wassilewskija. *Physiologia Plantarum* **129**(2): 342-350.

Schindfessel C, Jin C, Geelen D. 2022. Heat induced male meiotic restitution and sexual polyploidisation through natural variation of the Arabidopsis cyclin TAM/CYCA1;2. *BioRxiv*: 2022.2008.2011.503651.

Schulz E, Tohge T, Zuther E, Fernie AR, Hincha DK. 2015. Natural variation in flavonol and anthocyanin metabolism during cold acclimation in Arabidopsis thaliana accessions. *Plant, Cell and Environment* **38**(8): 1658-1672.

Sidhu GK, Fang C, Olson MA, Falque M, Martin OC, Pawlowski WP. 2015. Recombination patterns in maize reveal limits to crossover homeostasis. *Proc Natl Acad Sci U S A* **112**(52): 15982-15987.

Su H, Cheng Z, Huang J, Lin J, Copenhaver GP, Ma H, Wang Y. 2017. Arabidopsis RAD51, RAD51C and XRCC3 proteins form a complex and facilitate RAD51 localization on chromosomes for meiotic recombination. *Plos Genetics* **13**(5): e1006827.

Taghavi Namin S, Esmaeilzadeh M, Najafi M, Brown TB, Borevitz JO. 2018. Deep phenotyping: deep learning for temporal phenotype/genotype classification. *Plant Methods* **14**(1): 66.

Tang Z, Zhang L, Yang D, Zhao C, Zheng Y. 2011. Cold stress contributes to aberrant cytokinesis during male meiosis I in a wheat thermosensitive genic male sterile line. *Plant Cell and Environment* **34**(3): 389-405.

Vrielynck N, Schneider K, Rodriguez M, Sims J, Chambon A, Hurel A, De Muyt A, Ronceret A, Krsicka O, Mézard C, et al. 2021. Conservation and divergence of meiotic DNA double strand break forming mechanisms in Arabidopsis thaliana. *Nucleic acids research* **49**(17): 9821-9835.

Wang Y, Cheng Z, Lu P, Timofejeva L, Ma H. 2014. Molecular cell biology of male meiotic chromosomes and isolation of male meiocytes in Arabidopsis thaliana. *Methods Mol Biol* **1110**: 217-230.

Wang Y, Copenhaver GP. 2018. Meiotic recombination: mixing it up in plants. *Annual Review of Plant Biology* **69**: 577-609.

West AM, Rosenberg SC, Ur SN, Lehmer MK, Ye Q, Hagemann G, Caballero I, Usón I, MacQueen AJ, Herzog F, et al. 2019. A conserved filamentous assembly underlies the structure of the meiotic chromosome axis. *eLife* **8**.

Xue M, Wang J, Jiang L, Wang M, Wolfe S, Pawlowski WP, Wang Y, He Y. 2018. The number of meiotic double-strand breaks influences crossover distribution in Arabidopsis. *Plant Cell* **30**(10): 2628-2638.

Xue Z, Liu C, Shi W, Miao Y, Shen Y, Tang D, Li Y, You A, Xu Y, Chong K, et al. 2019. OsMTOPVIB is required for meiotic bipolar spindle assembly. *Proc Natl Acad Sci U S A* **116**(32): 15967-15972.

Yamamoto A, Hiraoka Y. 2003. Monopolar spindle attachment of sister chromatids is ensured by two distinct mechanisms at the first meiotic division in fission yeast. *Embo j* **22**(9): 2284-2296.

Yang C, Hamamura Y, Sofroni K, Böwer F, Stolze SC, Nakagami H, Schnittger A. 2019. SWITCH 1/DYAD is a WINGS APART-LIKE antagonist that maintains sister chromatid cohesion in meiosis. *Nature Communications* **10**(1): 1755-1755.

Yang C, Sofroni K, Hamamura Y, Hu B, Elbasi HT, Balboni M, Chu L, Stang D, Heese M, Schnittger A. 2022. ZYP1-mediated recruitment of PCH2 to the synaptonemal complex remodels the chromosome axis leading to crossover restriction. *Nucleic acids research* **50**(22): 12924-12937.

Yao Y, Li X, Chen W, Liu H, Mi L, Ren D, Mo A, Lu P. 2020. ATM promotes RAD51-mediated meiotic DSB repair by inter-sister-chromatid recombination in Arabidopsis. *Frontiers in Plant Science* **11**: 839.

Yuan G, Ahootapeh BH, Komaki S, Schnittger A, Lillo C, De Storme N, Geelen D. 2018. PROTEIN PHOSHATASE 2A B'α and β maintain centromeric sister chromatid cohesion during meiosis in Arabidopsis. *Plant Physiology* **178**(1): 317-328.

Zamariola L, De Storme N, Vannerum K, Vandepoele K, Armstrong SJ, Franklin FC, Geelen D. 2014. SHUGOSHINs and PATRONUS protect meiotic centromere cohesion in Arabidopsis thaliana. *Plant Journal* **77**(5): 782-794.

Zhang SS, Yang H, Ding L, Song ZT, Ma H, Chang F, Liu JX. 2017. Tissue-specific transcriptomics reveals an important role of the unfolded protein response in maintaining fertility upon heat stress in Arabidopsis. *Plant Cell* **29**(5): 1007-1023.

Zhao J, Gui X, Ren Z, Fu H, Yang C, Wang W, Liu Q, Zhang M, Wang C, Schnittger A, et al. 2023. ATM-mediated double-strand break repair is required for meiotic genome stability at high temperature. *Plant Journal* **114**(2): 403-423.

Zhou Q, Cheng X, Kong B, Zhao Y, Li Z, Sang Y, Wu J, Zhang P. 2022. Heat shock-induced failure of meiosis I to meiosis II transition leads to 2n pollen formation in a woody plant. *Plant Physiology* **189**(4): 2110-2127.

Zhu L, Fernández-Jiménez N, Szymanska-Lejman M, Pelé A, Underwood CJ, Serra H, Lambing C, Dluzewska J, Bieluszewski T, Pradillo M, et al. 2021. Natural variation identifies SNI1, the SMC5/6 component, as a modifier of meiotic crossover in Arabidopsis. *Proc Natl Acad Sci U S A* **118**(33).

Ziolkowski PA. 2023. Why do plants need the ZMM crossover pathway? A snapshot of meiotic recombination from the perspective of interhomolog polymorphism. *Plant Reproduction* **36**(1): 43-54.

Ziolkowski PA, Underwood CJ, Lambing C, Martinez-Garcia M, Lawrence EJ, Ziolkowska L, Griffin C, Choi K, Franklin FC, Martienssen RA, et al. 2017. Natural variation and dosage of the HEI10 meiotic E3 ligase control Arabidopsis crossover recombination. *Genes & Development* **31**(3): 306-317.

Supporting Information

Figure S1. Heat stress does not affect microtubule organization during prophase I in *Arabidopsis thaliana.*

Figure S2. Flower architectures in Col, L*er* and Col/L*er* hybrids.

Figure S3. Correlation analysis of synapsis, bivalent formation, and segregation of homologs at anaphase I in Col, L*er* and Col/L*er* hybrids.

Fig S4. Representative images of meiotic chromosomes from anaphase I to metaphase II in wild-type Arabidopsis.

785 Table S1. Primers used in this study.

786